DILEPTON AND PHOTON PRODUCTION
IN HIGH-ENERGY HEAVY-ION COLLISIONS

V.Emel'yanov, K.Haglin***

Physics Department, McGill University, 3600 University Street, Montreal P.Q. H3A 2T8, Canada

Electromagnetic signals provide useful means to track the space and time development of the dynamics in ultra-relativistic heavy-ion collisions. By themselves, they cannot be used to uniquely determine everything for these complicated systems, but they complement strong-interaction signals and are therefore quite valuable. Likely scenarios for time and distance scales relevant to these collisions, constituent identity and particle production are reviewed. Formalism for calculating photon and lepton pair production is presented, with an emphasis on recent developments.

Электромагнитные сигналы могут быть полезными для детектирования пространственно-временного развития динамических процессов в ультрарелятивистских столкновениях тяжелых инов. Сами по себе электромагнитные сигналы не могут быть использованы для однозначного определения динамики, но они существенно дополняют сигналы сильных взаимодействий. Рассмотрены наиболее вероятные сценарии пространственно-временной эволюции и рождения частиц. Рассмотрены современные методы расчетов спектров фотонов и лептонных пар.

1. INTRODUCTION

The development of Quantum Chromodynamics (QCD) over the last two decades or so can be divided in two general stages. The first is the study of «hard» processes. It is well known that the coupling constant of strong interactions, α_s, decreases with increasing squared transferred 4-momentum $|Q^2|$, owing to asymptotic freedom. For $|Q^2| \gg \Lambda_{QCD}^2$ ($\Lambda_{QCD} \sim 200$ MeV) the

*Permanent address: Department of High Energy Physics, Moscow Physical Engineering Institute, Kashirskoe Shosse 31, 115409, Moscow, Russia. Internet: vemel@hed.mephi.msk.su
**Present address: National Superconducting Cyclotron Laboratory, Michigan State University, East Lansing, Michigan 48824-1321, USA. Internet: haglin@theo03.nscl.msu.edu

coupling constant $\alpha_s \ll 1$, and calculations can be made within perturbative QCD. Such calculations have been carried out intensively over the last twenty years. The predictions of QCD were brilliantly confirmed, for example, by the experimental observation of hadronic jets with large transverse momenta.

But in quantitative comparisons with experimental data, some clean predictions of QCD perturbation theory are often lost in the maze of the phenomenology of soft processes. The point is that particles which are actually observed are not QCD quarks and gluons but hadrons resulting from soft processes of quark and gluon hadronization. By the early '80s, the QCD properties had been realized quite well within perturbation theory. It was perfectly clear, however, that perturbative QCD was far from exhausting the theory as a whole. Such fundamental properties of strong interactions as colour charge confinement, breaking of chiral invariance, and the hadron mass generation are due to nonperturbative fluctuations in QCD. Among theoretical methods of nonperturbative QCD, the following three have been intensively pursued: lattice gauge theory calculations, QCD sum rules, and quasi-classical (instanton) approaches. Some results obtained using these methods are discussed below. We would only like to mention here that the above schemes share the feature according to which the natural QCD vacuum state is appreciably distinct from the perturbative vacuum. How does the QCD vacuum change its state with increasing $\alpha_s(Q^2)$ and what are the consequences of this change? To be tackled, these complicated problems have to be considerably simplified. One may consider a macroscopic system of quarks, antiquarks and gluons which obey the laws of thermodynamics. At high temperatures, $T \gg \Lambda_{QCD}$, the characteristic momentum transfer in the interaction appears to be fairly large, $Q^2 \sim$ $\sim T^2 \gg \Lambda_{QCD}^2$, and the running coupling constant becomes small, $\alpha_s \sim$ $\sim 1/\ln(Q^2/\Lambda_{QCD}^2) \ll 1$. Owing to the asymptotic freedom of QCD, such a system is thus a relativistic gas of rather weakly interacting quarks and gluons, and these may propagate over distances greater than usual hadronic sizes. This new state of matter is the so-called quark-gluon plasma (QCD) [1]. A similar line of thought can be applied to states of relatively modest temperatures but high densitites.

The concept of hot hadronic matter was developed in some pioneering papers [2,3,4] where statistical and hydrodynamical methods were used to study ensembles of strongly interacting particles. But these authors were mainly concerned with hot and dense systems made up of hadrons[1]. Similar ideas are applied now, but additional features typical of QCD are incorporated. It has

---

[1]In this work we shall apply the terminology «hadron» to strongly interacting particles occuring in the non-perturbative sector of QCD.

been qualitatively predicted that QCD has a phase transition [5,6] and this prediction has later received support from early lattice gauge calculations [7]. The hadron-QGP transition temperature T_c appears to be of the order of 150—200 MeV and the QGP density to be several (~ 5) times the equilibrium nuclear matter density. But the situation of a possible phase transition is presently unclear and we will discuss this problem in detail below. For the moment it suffices to point out that the critical parameters, the order and even the existence of the QCD given phase transition are presently approach-dependent.

Since the expected temperatures $T \sim T_c \sim \Lambda_{QCD}$ belong to the QCD-infrared region, the majority of models [1] of macroscopic QCD systems are phenomenological in character. We may thus hope that precise experimental data will appreciably reduce the number of acceptable phenomenologies. Purely phenomenological approaches are useful but clearly unsatisfactory as they lack a truly fundamental basis. In this respect, the attempts to calculate the properties of strong-interaction thermodynamics starting from the fundamental QCD Lagrangian in lattice gauge theories are much more attractive, but these quickly run into technical problems of considerable complexity. Finally, concepts in finite-temperature and finite density QCD also carry cosmological and astrophysical consequences. Conditions typical of phase transitions in strongly interacting matter were probably realized immediately after the Big Bang and may still exist deep inside neutron stars. These questions are unfortunately beyond the scope of the present review, but interested readers may consult a detailed study in Ref.[8].

The interest in the thermodynamic aspects of QCD has increased recently because of the genuine experimental possibilities to study such extreme conditions by selecting specific events in hadronic collisions, more specifically in high energy heavy-ion collisions. It is quite amusing, that events as complicated as nucleus-nucleus (AA) collisions can be described in some respects more easily than nucleon-nucleon (NN) collisions, owing to the power and elegance of statistical and thermodynamic approaches. Therefore, the subject of heavy-ion collisions is intimately connected to the study of bulk matter properties for systems consisting of strongly interacting particles (hadrons or partons). The above line of reasoning in the investigation of nuclear matter under extreme conditions does not imply, however, that a phase transition must necessarily take place in high energy AA collisions. It is also not *a priori* clear whether or not local thermodynamic equilibrium in strongly interacting matter is established and thus whether or not it is possible to describe such a system within a thermodynamic approach. The answer depends on the relation between the characteristic time τ_i of establishing local thermodynamic equilibrium and characteristic time $\tau_{react.}$ of heavy-ion reactions. The time needed to establish local

Table 1

Time	Machine	Beam	CMS Energy (GeV/nucleon)
1986—1993	BNL-AGS	up to ^{28}Si	5
	CERN-SPS	up to ^{32}S	20
1993—1998	AGS + booster	all A	4 (Pb)
	SPS + Pb injector	all A	17 (Pb)
1998—	RHIC	all A	200 (Pb)
	LHC	all A	6300 (Pb)

thermodynamic equilibrium was originally estimated [9,10] to be $\tau_i \simeq 1$ fm/c. But these early estimates, in our opinion, can only be trusted to within an order of magnitude. If $\tau_i \simeq 10$ fm/c, this means that local thermodynamic equilibrium is extremely unlikely in such collisions. The theoretical question of establishing local thermodynamic equilibrium in a system of interacting hadrons has no single answer at the present time. This is however a crucial point for the understanding and the description of hadronic matter in collision. We believe that the tools to tackle this problem experimentally now exist. Furthermore, we shall describe some recent results that bring credibility to the notion of early equilibration times.

Another important practical question is: what energy densities and nuclear matter temperatures can be attained in existing and future heavy ion accelerators? In Table 1 we summarize the present status and the future plans for heavy ion experiments.

Up to very recently, the existing sources and existing accelerators had collimated and accelerated rather light ion beams (up to ^{32}S and ^{28}Si). It is expected that soon, both the BNL-AGS and the CERN-SPS (also RHIC and the LHC in 1998) will have new injectors able to accommodate very heavy ions, all the way up to uranium. The first Au-Au experimental run has in fact been taken at the BNL-AGS accelerator. This global program will make it possible to determine to what extent we can actually get into a regime of thermodynamic behaviour. If in these experiments, one can obtain sufficiently high initial temperatures and/or initial densities, a study of the properties of the quark-gluon plasma should become possible. But if $T_i < T_c$ or $n_i < n_c$, one will likely obtain only hadronic plasma. However, we hope to convince the reader that the study of the properties of the latter is perhaps as interesting as that of the QCD plasma! Below, we will try to estimate T_i and n_i at present and future accelerators.

If a quark-gluon or an hadronic plasma is formed in heavy-ions collisions, what are its experimental signals? It is fair to say that at present there is no single answer to this question. In the strong sector, the onset of thermalization may be tested by studying strangeness away from the *NN* level, for kaons as well as hyperons [11,12,13]. Here as elsewhere, the main difficulty in the identification of hot matter signals is that the background from «ordinary» hadronic sources is typically not small. Possible signature candidates considered are: (1) discontinuities in the momentum distribution of the secondaries, reflecting a «hadron quark-gluon plasma» first-order phase transition [14]; (2) particle ratios which are significantly different for a hadron gas than they would be for a hadronizing quark-gluon plasma [11,13]; and (3) droples of strange matter, baryonic states of very low charge to mass ratio [15]. But these strong probes all have an obvious disadvantage: the soft process of hadronization may substantially distort the information of hadronic system evolution. Furthermore, they might just reflect the state of the system at freeze-out.

Leptons and photons have small cross sections strongly interacting matter, and so their mean free paths are typically much larger than the transverse size of the region of hot matter created in a nuclear collision. As a result, high energy leptons and photons produced in the interior of the plasma will typically pass through the surrounding matter without interacting, carrying information directly from wherever they were formed formed to the detector. It is quite natural that leptons and photons have been considered [16—24] as an outstanding tool in the search for hot nuclear matter and the quark-gluon plasma. The topic of our review is dilepton and photon production in high energy heavy-ion collisions. We will not discuss the topic of dilepton and photon production at low-to-moderate energies ($E \le 10$ GeV/nucleon corresponding to Bevalac and GSI energies). For a review of the experimental data and the theoretical models in this energy regime, the interested reader should consult Refs. [25—27]. We will consider the following questions: What information about hot and dence strongly interacting systems can be carried by the lepton and photon spectra? What are the sources of lepton and photon production? In a partial answer, we state that the problem of lepton and photon production is intimately connected with the behaviour of quarks, gluons and mesons in hot and dence matter. For example, there might be collective resonance effects which will influence the dilepton and photon spectra. Qwing to scattering processes, the positions and widths of ordinary propagating mesons are also potentially modified. We shall insist on the fact that the study of electromagnetic radiation from heavy-ion collisions at high energies offers unique insights in the many-body problem of the strong interaction at finite temperatures and densities.

The paper is organized in the following way. Section 2 is devoted to modern calculations of critical temperature and density of phase transition in lattice gauge theories. We also discuss the order of phase transition, screening

lengths and non-perturbative effects. In section 3 we describe space-time evolution of hadronic matter and estimate the initial energy density in relativistic heavy-ion collisions. Section 4 is devoted to the calculations of dileptons and photons spectra from QCD and hadronic gas. We discuss also the spectra properties. In Section 5 we give a short conclusion.

2. PHASE TRANSITION IN LATTICE GAUGE THEORIES AT FINITE TEMPERATURE

Successful calculation of physical quantities, including those in the strong coupling regime of QCD have been carried out in the last decade within the framework of lattice gauge theories (LGT) [28,29]. The advantages of this method are obvious because the calculations are based on the QCD Lagrangian itself and not on some of its phenomenological extensions. However, the calculations are performed by Monte Carlo methods wherin one is not always successful in following the gauge field dynamics. In LGT, continuous space-time is replaced by a lattice in Euclidean space with N_σ sites in each space direction and N_β sites in each time direction. The state of the lattice is characterized by a fixed set of matrices «u» on the links, and quark states on sites. A lattice is a statistical system.

In the simplest case of gluo-dynamics (quark-free QCD) the lattice partition function has the form

$$Z(z, N_\sigma, N_\beta, g^2) = \int \Pi dU \exp(-S(\{u\})), \qquad (1)$$

where $z = a_\sigma/a_\beta$ and a_σ, a_β are distances between neighbouring lattice sites in the space and time directions, ΠdU is the product of Haar measures corresponding to functions that realize the gauge group representations, $S(\{u\}))$ is the action [28,29] which depends on the gauge field values and on the links of squares (the so-called plaquettes) of the lattice in the space and time directions. The expectation value of the physical quantity X is determined using the partition function:

$$<X> = \int \Pi dU X(\{u\}) \exp(-S(\{u\})) / \Pi dU \exp(-S(\{u\})). \qquad (2)$$

In LGT such expressions are numerically integrated by Monte Carlo methods. Lattice calculations are also used to study QCD at finite temperatures. Here it is necessary to restrict the «size» of the system to $N_\beta a_\beta = = 1/T$ in the imaginary time direction. T is the system temperature.

Let us now discuss the results of calculatins of the most interesting physical quantities. Among the quantities which are studied in high temperature QCD are the Polyakov loop, the chiral condensate $< \overline{\psi}\psi >$, the energy and pressure, the screening lengths of colour singlet sources, the potential between static test quarks and the responce of the quark density to an infinitesimal chemical potential. Of these, the Polyakov loop and $< \overline{\psi}\psi >$ are the most studied. $< \overline{\psi}\psi >$ is the order parameter for chiral symmetry breaking. It is nonzero under ordinary conditions, and it vanishes when chiral symmetry is restored. Loosely speaking, the Polyakov loop is $\sim \exp{(-F/T)}$, where F is the free energy of a static test quark. In pure glue QCD, the Polyakov loop is zero at low temperatures, indicating confinement of the test quark, and nonzero at high temperatures, indicating deconfinement. One can observe the crossover to high-temperature behaviour in lattice simulations. To vary the temperatures with a fixed number of lattice sites in the time direction, one can vary the lattice spacing a_β by varying the coupling g. Then, decreasing g, or increasing $6/g^2$, makes a_β smaller and the temperature, $T = 1/N_\beta a_\beta (g)$, higher. As the temperature is increased, $< \overline{\psi}\psi >$ drops and the value for the Polyakov loop increases. The Polyakov loop and $< \overline{\psi}\psi >$ undergo rapid changes around the same temperature, indicating that deconfinement and chiral symmetry restoration are happening at the same temperature. However, this does not really confirm or exclude the case with $T_{dec} = T_{chiral}$. We have so far considered a simplified QCD (with a quark-free gauge group). In the more realistic situation — the gauge group SU(3) and quark degrees of freedom — LGT runs into a number of difficulties [29]. The main difficulty is to correctly account for virtual quark-antiquark loops in Monte Carlo methods. This is a topic of current research in LGT.

Figure 1 shows a crude phase diagram of QCD as a function of quark mass and temperature. For infinite quark masses the quarks are never excited and we have quenched, or pure glue, QCD. In this case, it is fairly well established from lattice simulations that there is a first-order phase transition [30]. As the quark mass is lowered from infinity, this transition disappears. Although there is no phase transition, the crossover is still fairly sharp.

In Fig.2 [31] we show the inverse screening lengths for sources with the quantum number of the pion and its parity-partner. At high temperatures the two become very close, with the remaining difference being due to the explicit symmetry breaking by the quark mass. This quantity shows that the high temperature regime has the expected characteristics of the quark-gluon plasma.

With four flavours of quarks it seems that a first-order transition reappears when the quarks are very light [32—41]. For two flavours of light quarks or two light quarks and a strange quark, there is no evidence for a phase transition. Several groups have studied this over the last few years and the consensus is
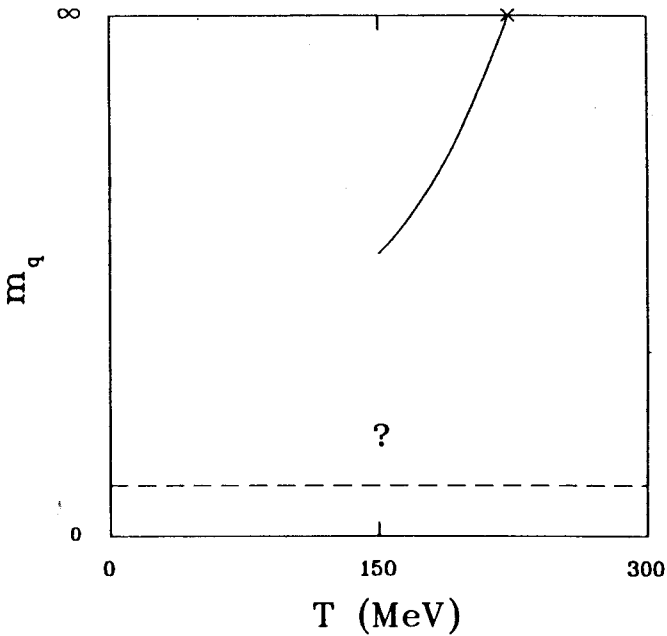
Fig. 1. Phase diagram of QCD as a function of quark mass and temperature

that with the quark masses being used in these calculations, the crossover is smooth. The Illinois and Columbia groups have studied two light flavours plus one heavier flavour [37,38]. They did not find evidence for a phase transition. It may be that with two light flavours the transition is second order for quark

Table 2

Flavour	T_c (MeV)	Reference
0	200—220	[41]
2	140—150	[32,42,43]
2 + 1	140	[39]
4	100—110	[44]
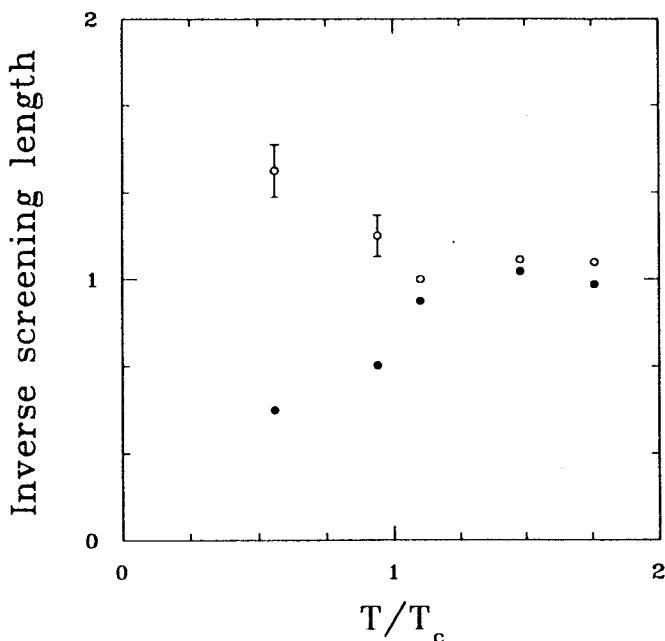
Fig.2. Inverse screening lengths for sources with the quantum numbers of the pion and its opposite parity partner as a function of temperature. Solid squares are the pion (O^-) screening mass and open circles are sigma (O^+) screening mass

mass exactly zero with only a rapid crossover for finite quark mass, as suggested by a renormalization group analysis [39]. To find the temperature of the crossover in physical units, it is necessary to determine the lattice spacing by computing some physical quantity, such as the rho or nucleon mass. The estimates summarized in Table 2 are obtained when the rho mass is used to set the scale. The pion mass is not a good choice in general, since it can be made arbitrary small by making the quark mass small. If the nucleon mass is used, all of these temperatures decrease by about 20 %. Notice that these estimates are lower than those from most phenomenological models of the hadronic and plasma phases [1,45].

Figure 3 summarizes the dependence of the QCD phase transition on the number of light quark flavours [38]. The line along the top of the figure $(m_s = \infty)$ corresponds to the two-flavour case and has a second order critical
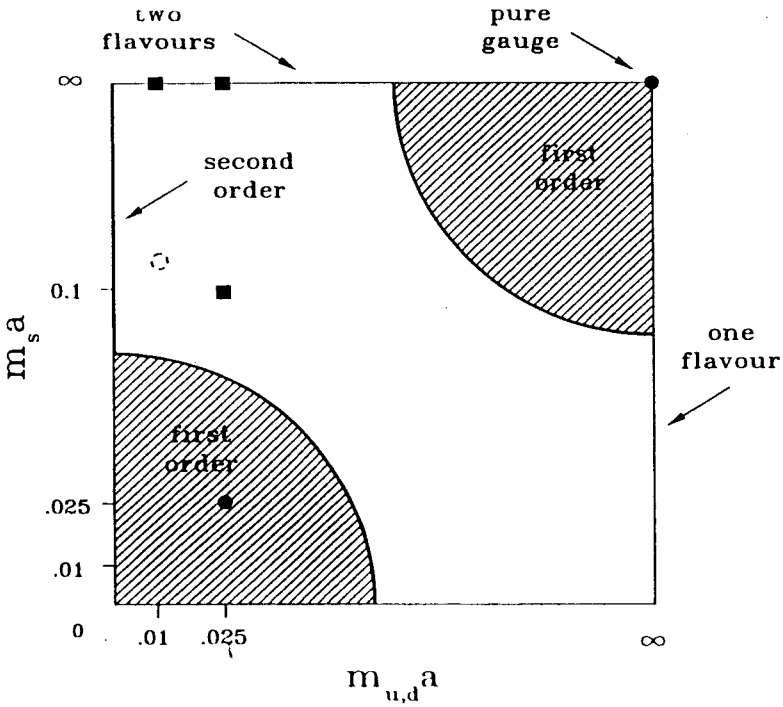
Fig.3. Phase structure of QCD as a function of the u, d and strange quark masses. The points denote regions where calculations have been done and where the transition is seen (solid circles) and not seen (solid squares). The dashed circle is the physical point (from Ref. [38])

point when $m_{u,d} = 0$. The physical situation with two light u and d quarks and a considerably heavier s quark appears to lie on the borderline between first order and crossover behaviour.

The question of the order of phase transition (or of the absence of phase transition) is not only of theoretical but also of practical interest. Indeed, in the case of first-order transition a system of hadrons, quarks and gluons can be in a mixed phase at a temperature T_c. Under a second-order transition, the «QGP-hadron» transition occurs rapidly at a temperature T_c. This fact is quite important in any experimental diagnostic of QGP production.
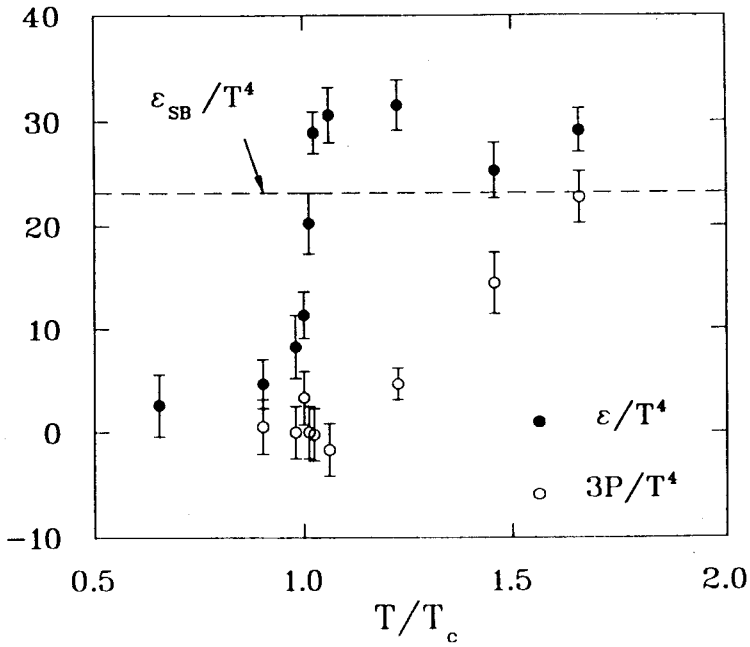
Fig.4. Energy density and pressure of QCD matter as a function of temperature

The order of the phase transition is at present under intense investigation by lattice studies. One finds a first-order deconfinement transition for $N_f = 0$ and a first-order transition corresponding to chiral symmetry restoration and deconfinement for $N_f \geq 3$ in the limit of massless quarks (see discussion in Ref. [46]). For $N_f = 2$ there is a second-order transition in the case of massless quarks (Fig.3) and a strong crossover behaviour for non-zero quark masses. However, for two light and one heavy quark the situation appears to lie between a first-order phase transition and a crossover behaviour. All results at vanishing baryon number density seem to agree on the fact that the transition point for deconfinement and chiral symmetry restoration are consistent with each other.

In Fig.4 we show the behaviour of the QCD energy density and the pressure for matter with two flavours of light quarks (u and d) [34]. As one can see, at a critical temperature T_c, the energy density undergoes a rapid transition from low values, corresponding to a hadron gas, to much higher values (Stefan-Boltzmann limit ε_{SB}), corresponding to a quark-gluon plasma. The energy density of
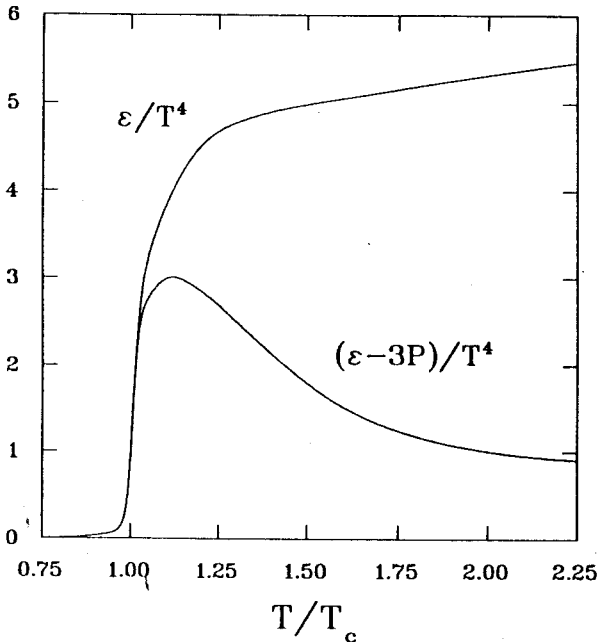
Fig.5. Energy density ε and «interaction strength» $(\varepsilon - 3P)/T^4$ in SU(3) gauge theory as a function of temperature

an ideal plasma with finite-size lattice corrections [47] is also shown in Fig.4. At high temperatures $(T/T_c \geq 2)$ the calculations appear to approach this value. As is well known, the energy density and pressure are related by $(\varepsilon - 3P)/T^4 = 0$ for an ideal plasma. We see that this condition is certainly not fulfilled for $T \leq 1.5T_c$: below $1.5T_c$ the energy density approaches the Stefan-Boltzmann limit and the pressure falls much below the ideal limit.

The energy density ε and the «interaction strength» in SU(3) gauge theory are plotted as a function of the temperature T, in Fig.5 [48]. This indicates that the system will not become ideal until temperatures become quite high.

As in ordinary electron-positron plasma, a screening length can also be defined in the QGP. In connection with this, we will mention the suppression of the J/ψ in heavy-ion collisions. One can imagine that bound states (such as $c\bar{c}$ or $b\bar{b}$) will «melt» in dense matter when the screening radius becomes significantly smaller than the binding radius. The temperature dependence of the Debye screening radius $r_D(T)$ gives us some idea of when specific bound states
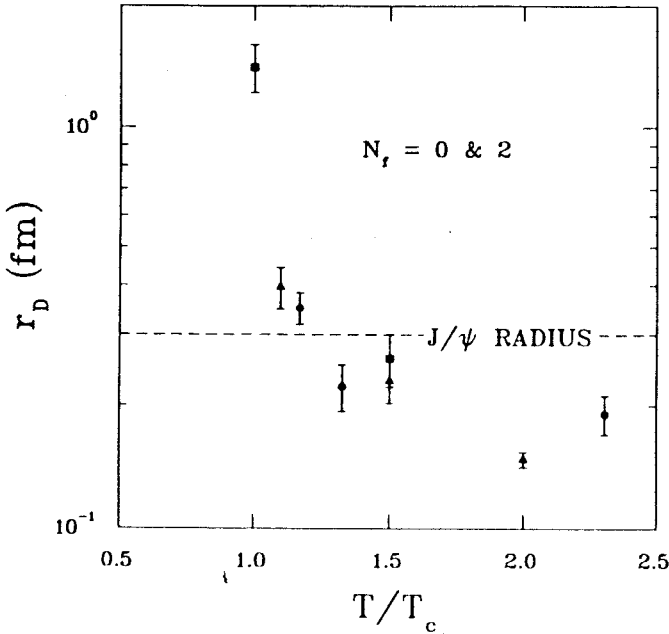
Fig.6. Colour screening radius r_D as a function of the temperature T for QCD matter ($N_f = 0$ & 2)

will disappear. From Fig.6 [49] we see that above $T \simeq 1.2T_c$, the tightly bound $c\bar{c}$ state we known as J/ψ should become unbound.

Simulations of lattice QCD have shown that chiral symmetry is restored at high temperatures, as indicated by the vanishing of the order parameter $\langle\bar{\psi}\psi\rangle$. Additional evidence for the restoration of chiral symmetry can be obtained by using hadronic correlation functions [50]. The exponential falloff of such correlation functions at large spatial separations determines screening lenghts. Unbroken symmetries are reflected in degeneracies of the screening lengths. Another reason to study the hadronic correlations is to try to extract information about possible hadronic real time modes in the high temperature phase. The extracted screen masses { $=$ (screening length)$^{-1}$ } can be compared with the corresponding values for a gas of free quarks. Already at $T = 1.5T_c$, the screening masses associated with vector fields are close to their free values. For temperatures higher than $T = 1.5T_c$, lattice results [51] suggest that $q\bar{q}$ and qqq states propagate like weakly interacting quarks rather than as bound states.

Summarizing, it seems that lattice data give reasonably strong evidence for the existence of a phase transition (first, weak first or second order) in strongly interacting matter at temperatures $T_c \simeq 140$—200 MeV and energy densities $\varepsilon_c \simeq 1$—3 GeV/fm^3. Also, the properties of a quark-gluon plasma or an hadronic gas near T_c are quite different from that of completely non-interacting systems. A final word of warning: the lattices in current use are still reasonably coarse. This aspect is however continuously being improved upon.

3. SPACE-TIME EVOLUTION
OF HEAVY-ION COLLISIONS

It is not at all clear that the considerations of the previous section are at all relevant in the context of heavy-ion collisions. Apart from the equilibrium requirements (which we discuss in more detail below), we have already mentioned the difficulties that finite-temperature LGT has in making contact with physical observables. Let us then turn to more phenomenological aspects of the problem at hand, adopting however LGT as a formal backdrop to our discussions.

Before proceeding to nucleus-nucleus collisions, we recall a simpler space-time picture: one of hadron-hadron interactions. In the framework of the quark-parton model of hadrons, the interaction of hadrons in the high energy region is assumed to proceed as follows:

a) Before collision, relativistic hadrons are ensembles of partons (valence quarks, sea quarks, antiquarks, and gluons) properly distributed with respect to the hadron momentum fraction x, carried by them. The initial distribution functions of partons can be derived from the experimental data on deep inelastic eN, μN, νN, or $\tilde{\nu} N$ interactions.

b) As a result of hadron-hadron interaction, some of the fast partons do not participate in collective interaction and, under hadronization, subsequently form leading secondary hadrons. Comparatively slow partons of colliding hadrons interact with one another forming a quark-gluon system whose evolution results in the formation of the soft part of the secondary hadron spectrum.

What do we expect, going from hadron-hadron to nucleus-nucleus collisions?

First of all, nuclei are extended objects, and therefore their geometry plays an important role in heavy-ion collisions. The time scale for such collisions is much greater than in hadron-hadron interactions, and this can lead to interesting phenomena. The space-time evolution of a central (impact parameter $b = 0$) Pb-Pb collision at very high energies (RHIC, LHC) is show schematically in Fig.7.
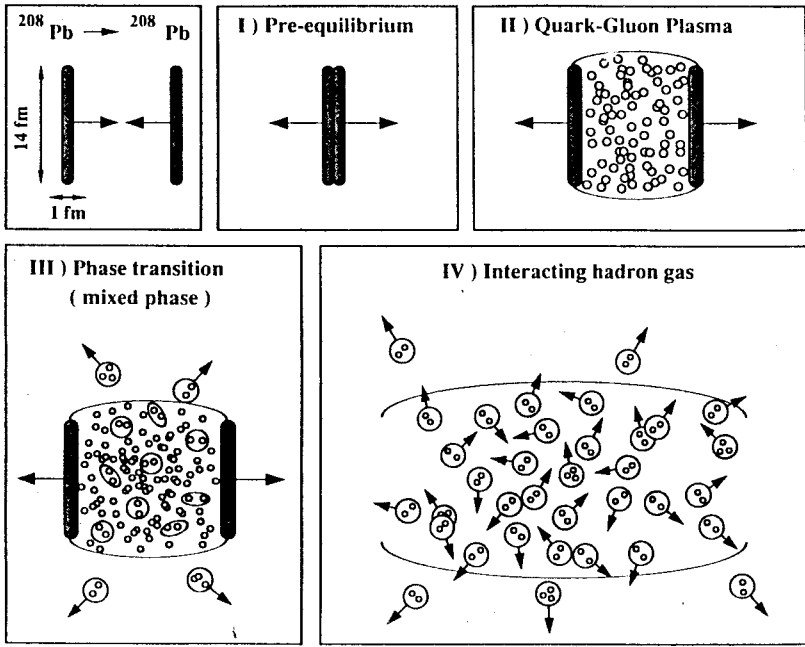
Fig.7. Space-time evolution of Pb-Pb interactions

In the first moments of interaction, nucleon-nucleon collisions between the two highly Lorentz-contracted nuclei (with thickness $\simeq 1$ fm/c) redistribute a fraction of the initial beam energy into other degrees of freedom. After a short time (we will discuss this time below) partons materialize out of the highly excited QCD field. This is the preequilibrium state of QCD matter. Under certain conditions, multiple parton-parton collisions at this stage can lead to establishing a local thermodynamic equilibrium in quark-gluon systems at an initial temperature T_i. As discussed previously, if the local energy density is high enough, QGP is formed. The QGP expands rapidly, mainly along the longitudinal direction, lowers its temperature and reaches the critical transition temperature T_c. If phase transition is first order, the matter spends some time in the mixed phase, in which there coexist quarks, antiquarks, gluons and hadrons. It rearranges the many degrees of freedom of the QCP into the small number available in the hadronic phase with a large associated release of latent heat. In its ultimate phase (hadron gas or hadron fluid), the still-interacting system keeps expanding until «freeze-out», when interactions cease and the particles stream freely away to be detected in the experiments.

In this approach to the problem, two important questions immediately arise:

1. How should one describe the transition of a quark-gluon system from the initial state (before hadron collisions) to the state of thermodynamic equilibrium?

2. Is local thermodynamic equilibrium of the hadronic matter established in reality? In other words, might the entire nucleus-nucleus process be described on a microscopic level (in terms of the distribution function of partons) or does there exist a time interval when a macroscopic (statistical) approach can be applied to the quark-gluon system evolution? At first glance, a rather large amount of mutual collisions of partons is required to attain thermodynamic equilibrium. For example, according to Ref.[52], this number ≥ 10. But the number of mutual collisions of partons is not the only relevant factor for the formation of local thermodynamic equilibrium. One should bear in mind that QCD partons are carriers of colour degrees of freedom. Therefore, already at the initial stage of interaction, parton distribution over x can be described by a superposition of collective and «internal» (colour) states [53]. Thus, if at the initial stage of hadron-hadron collisions, colour degrees of freedom are excited and statistical averaging is carried out over these degrees of freedom, then the conditions for the collective (hydrodynamic) behaviour of the parton system can also be realized when the number of parton-parton collisions is small ~ 2—3 [53].

The time for establishing local thermodynamic equilibrium has been estimated [9,10] to be $\tau_i \simeq 1$ fm/c. However, we believe it is fair to say that the concept of a local thermodynamic equilibrium in the collision of large nuclei at ultrarelativistic energies is still not firmly supported by theory nor experiment.

Among the attempts to theoretically describe the kinetic processes responsible for an eventual relaxation to equilibrium state one should mention Refs.[54—56]. In these works the initial conditions in hadron-hadron collisions are given by the structure functions of the colliding hadrons. During individual hadron-hadron collisions, new partons are created in addition to those that already existed in the incoming hadrons. The repeated collisions between partons substantially affect their structure functions. This approach is essentially kinetic and can describe experimental data on hadron-hadron interactions, provided one has chosen suitable «initial» structure functions.

Other attempts to quantitatively describe the kinetic stage of hadron-hadron (or nucleus-nucleus) collisions were made in Refs.[57,58]. In the CMS of two colliding hadrons their interaction can be treated as a result of exchange with one or more gluons, which leads to a nonzero effective colour charge of the hadrons. In this process a chromoelectric tube occurs which is unstable under quantum creation of quark-antiquark pairs and gluons. The produced $q\bar{q}$ pairs and gluons interact among themselves and with the chromoelectric field, and if

the characteristic times of strong interactions exceed the collision times of the produced $q\bar{q}$ pairs and gluons, then the system of quarks, antiquarks and gluons can be brought into a state of local thermodynamic equilibrium.

The important program to study partonic cascades, tracing the system all the way from the structure functions to an equilibrated QGP, has recently been undertaken [59,60,61]. The nuclear collision is described as a sequence of multiple hard and soft parton-parton collisions and associated parton emission and absorption processes. Important aspects for the space-time evolution of the partonic system are the detailed balance between emission and absorption processes, the treatment of the Landau-Pomeranchuk effect, and the effects of soft gluon interference. In this approach, a cut-off is chosen to separate between «soft» and «hard» QCD processes. The location of this cutoff is still an open problem in this approach. The time during which most of the entropy is produced was found to be $\tau \simeq 1/2$ fm/c for RHIC conditions, momentum distributions approach thermal ones and gluons clearly outnumber quarks. These results have essentially supported the «hot-glue» scenario [62]. Using the lowest order perturbative QCD, E.Shuryak argued that high energy heavy-ion collisions proceed via two stages: equilibration of gluons takes time $\tau_g \simeq 1/2$ fm/c, while production and equilibration of quarks needs at least $\tau_q \sim 2$ fm/c. The initial temperature in the «hot-glue» scenario is $T_i \simeq 400$—500 MeV, a value much greater than in the «standard» scenario of complete equilibration of QGP at the time $\tau_i \simeq 1$ fm/c. In the latter case the estimated initial temperatures [63] should be $T_i \simeq 240$ MeV for RHIC conditions and $T_i \simeq 290$ MeV for LHC. Consequences of the «hot-glue» scenario on dilepton emission will be discussed in the upcoming chapters.

Other approaches of the non-equilibrium type are typified in the independent string model (ISM) [64]. The ISM assumes the absence of final state rescattering, i.e., particles produced in one string interact neither with particles produced in a different string nor with nucleons of the colliding nuclei. These models are theoretically consistent (unitary, analyticity, etc.), and have good predictive power in terms of rapidity distributions, nuclear stopping power, multiplicity and E_T distributions. However, it is easy to see that an energy density of 1 GeV/fm^3 is equivalent to a string density of 2 strings/fm^2, since each string has a «plateau» of about 1.5 particles per unit rapidity including neutrals, and each particle has a transverse energy of about 0.35 GeV. Therefore, string-string interactions seem unavoidable. Some recent scenarios attempt to incorporate this feature at the phenomenological level.

We shall mostly concentrate on approaches where thermodynamical equilibrium is assumed in the strongly interacting systems. In most applications, this can be done without any loss of generality. The state-of-the-art numerical

simulations based on a relativistic kinetic theory of parton cascades mentioned above also support this idea.

3.1. One-Dimensional Hydrodynamic Model of Evolution.

Formed at initial temperature T_i and energy density ε_i, QGP expands and cools. This process is naturally described with the equations of motion for an ideal relativistic liquid [65]. The hydrodynamic expression for conservation of energy and momentum is

$$\partial^\mu T_{\mu\nu} = 0 \,, \tag{3}$$

where the stress tensor $T_{\mu\nu}$ for a perfect liquid is

$$T^{\mu\nu} = (\varepsilon + p)\, u^\mu u^\nu - p g^{\mu\nu} \,, \tag{4}$$

$g^{\mu\nu}$ is the Minkowski metric, ε and p are the energy density and pressure in the co-moving frame, and u_μ is the matter collective four-velocity. Equations (3) and (4) imply $\partial_\mu s^\mu = 0$, where $S^\mu \equiv \sigma u^\mu$ is the entropy current.

In order for these partial differential equations to be closed, one must introduce an equation of state (EOS). The most widely used EOS for the quark-gluon plasma comes from the bag model [66]. For a baryonless plasma the energy density, entropy density and pressure are given by

$$\varepsilon_q = \frac{\pi^2}{30} d_q T^4 + B \,,$$

$$S_q = \frac{4\pi^2}{90} d_q T^3 \,,$$

$$P_q = \frac{\pi^2}{90} d_q T^4 - B \,, \tag{5}$$

where B is the usual bag constant and d_q is the number of degrees of freedom in the QGP. Usually the hadron phase is considered as a gas of noninteracting massless pions for which the ideal equation of state (IEOS) is

$$\varepsilon_\pi = \frac{\pi^2}{30} d_\pi T^4 \,,$$

$$S_\pi = \frac{4\pi^2}{90} d_\pi T^3 \,,$$

$$P_\pi = \frac{\pi^2}{90} d_\pi T^4 \,, \tag{6}$$

where d_π is the degeneracy factor for pions. However, the hadron phase is not a massless pion gas but a system of different kinds of massive hadrons. In Ref.[67], a more realistic equation of state (REOS) was introduced treating hadronic matter as a system of several species of extended massive hadrons [68]. The main difference in the hydrodynamic expansion for the IEOS and REOS is in the space-time volumes of the mixed and hadron-gas phases. In the case of IEOS, the system spends much of its time mixed phase and the hadron gas is less important. Whereas, with the REOS the system spends most of the time in the hadron phase and the mixed phase therefore plays a lesser role. We will discuss later how these differences affect the electro-magnetic signal.

Besides the equation of state, the determining role in the model predictions that fixes a unique solution of the hydrodynamic equations is played by the choice of initial (boundary) conditions. For example, Landau hydrodynamics [69] begins with the premise that in the CMS, the Lorentz-contracted nuclei approach each other, stick together and generate hot dense matter. Entropy generation, which ultimately governs particle production, occurs through the passage of a shock wave during the fusion. This is also the mechanism for heating the matter [70]. While this model takes into account the leading particle effect [71] and has other nice features, the energy density in the initial stage appears quite large. Hadron-nucleus collisions show that nuclei may be trans-parent to energetic hadrons and it has therefore been proposed [72] that nuclei at high energies may pass through each other. The initial conditions prescribed by Landau may not be so appropriate for ultra-relativistic heavy-ion collisions.

A simple yet powerful picture of hadronic matter evolution is provided by one-dimensional hydrodynamic expansion in scaling variables [73]

$$\tau = \sqrt{t^2 - z^2}, \tag{7}$$

$$\chi = \frac{1}{2} \ln \left(\frac{t+z}{t-z} \right). \tag{8}$$

Here t and z are the time and spatial coordinates of one-dimensional expan-sion in the CMS. In these variables, using the initial velocity distribution determined by a rapidity plateau

$$Y(\chi, \tau = \tau_i) = \begin{cases} \text{const}, & |\chi| \leq Y_m \\ 0, & |\chi| > Y_m \end{cases}, \tag{9}$$

the solution of the equations of one-dimensional hydrodynamic expansion is especially simple (scaling solution) [9,74]. The temperature turns out to be only a function of the proper time τ of the hadron liquid element, i.e.,

$$T(\chi, t) = T(\tau) \tag{10}$$

and not of the variable χ. The rapidities of the elements are in turn determined only by the variable χ

$$Y(\chi, t) = \chi. \tag{11}$$

Correspondingly, the velocities of matter elements are given by

$$\upsilon(\chi, t) = \frac{z}{t} = \tanh \chi. \tag{12}$$

A schematic picture of hadronic matter evolution in these variables is presented in Fig.8. In the region $0 \le \tau \le \tau_i$ hadronic matter is in the preequilibrium phase, then for $(\tau_i < \tau < \tau_q)$ there exists an equilibrium QGP phase followed by a mixed phase region, and finally a hadron liquid (gas). At $\tau = \tau_f$ the system decays into observed secondary hadrons. It can be readily seen that the scaling solution leads to scale-invariant spectra of secondary particles distributed over rapidites in accordance with a Feynman plateau. From Fig.8 one can imagine how difficult it is to detect QGP experimentally. Indeed, the QGP lifetime is only $\tau = \tau_q$, which may be much smaller than the time τ_f (see below). The QGP formation signal will therefore be obscured by emission from preequilibrium, hadron and mixed phases.

Of course, this one-dimensional model of nuclear matter evolution must be considered only as a «first approximation» to real nuclear matter evolution in heavy-ion collisions. Certaintly, the evolution is not one-dimensional at the latter stages of evolution. But cascade model simulations [60] show that during the first 3 fm/c the system of partons expands exclusively in the longitudinal direction, i.e., along the z axis. All volume elements expand approximately linearly with time and more in straight lines from the collision point at $z \simeq 0$ with flow velocities that increase from the slowest expansion in the center of mass at $z = 0$ up to the speed of light in the fragmentation region of the receding beam fronts.

3.2. Initial Energy Density of Thermalized Hadronic Matter. Let there occur a central collision of two identical nuclei with mass numbers A, which move in the CMS with a Lorentz factor γ ($\gamma = E / m \gg 1$, where m is the nucleon mass and E is the energy per nucleon). In the longitudinal direction, nuclei experience Lorentz contractions down to sizes $2R_A / \gamma \simeq 2A^{1/3} / m_\pi \gamma$ (R_A is the radius of the nucleus with mass number A and m_π is the mass of the π-meson). Let us evaluate the energy density at the moment of establishing thermodynamic equilibrium for an hadronic cluster of thickness $2\Delta x$ between two boundaries —
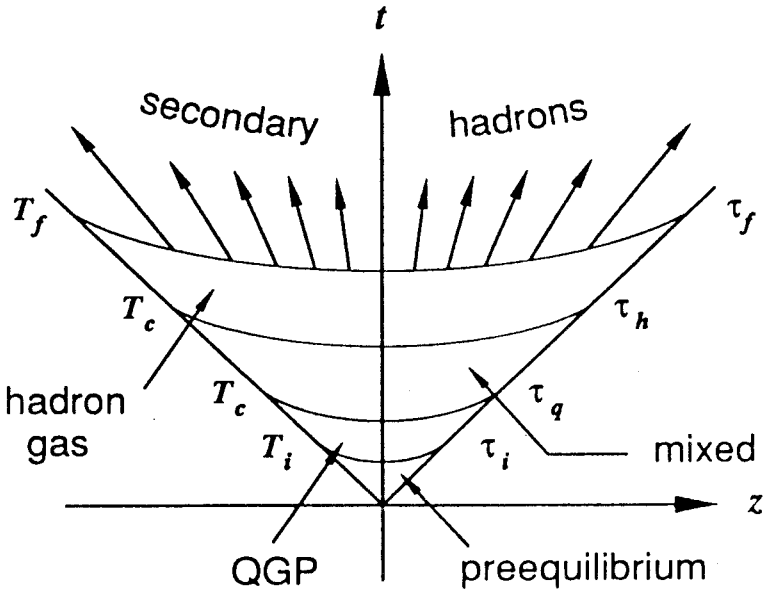
Fig.8. Space-time evolution of hadronic matter in one-dimensional hydrodynamic model

flat layers — moving at velocities $\upsilon = \pm \Delta x / \Delta t$. According to the scaling solution, the secondary hadrons corresponding to this layer will be bound within the rapidity interval $\Delta y = 2$ arctanh $(\Delta x / \Delta t) \simeq 2\Delta x / \Delta t$. In the approximation of noninteracting secondary hadrons, the energy in the layer will be

$$E = A \frac{d \langle E \rangle}{dy} \Delta y. \tag{13}$$

To determine the initial energy density ε_i, one must simply divide the energy by the initial volume, $\varepsilon_i = E / V_i$. The cluster volume at the moment of thermalization τ_i is conveniently written using the scaling variables, where an element of 4-volume is

$$d^4 x = d^2 x_t \, d\chi \tau d\tau. \tag{14}$$

Integrating over χ with limits $\pm \Delta y / 2$, we find

$$V_i = \pi R_A^2 \tau_i \Delta y, \tag{15}$$

where πR_A^2 is the cross-section of the colliding nuclei, $\pi R_A^2 = 4.5 \text{ fm}^2 A^{2/3}$. Then the initial energy density is [9]

$$\varepsilon_i \simeq \frac{A^{1/3}}{4.5 \text{ fm}} \frac{d\langle E \rangle}{dy} \frac{1}{\tau_i}. \tag{16}$$

If we approximate charge densities in central heavy-ion collisions by

$$\left(\frac{dN^{ch}}{dy} \right)_A = A^\alpha \left(\frac{dN^{ch}}{dy} \right)_P, \tag{17}$$

with $(dN_{ch}/dy)_P$ being the charged-particle multiplicity in pp collisions (present data from nuclear collisions suggest $\alpha \geq 1.1$), then the initial energy densities are

$$\varepsilon_i \simeq 0.09 A^{\alpha - 2/3} \ln \sqrt{s} \tag{18}$$

if we use $\tau_i \simeq 1$ fm/c.

From this formula we obtain for central Pb-Pb collisions

	ε_i (GeV/fm^3)
SPS	2.5
RHIC	4.7
LHC	8.0

For an ideal QGP with three flavours of masselss quarks [75]

$$\varepsilon = \left(\frac{47.5 \, \pi^2}{30} \right) 8 T^4, \tag{19}$$

which leads to an initial temperature $T = (\varepsilon / 1953)^{1/4}$ (with ε in GeV/fm^3 and T in GeV). For Pb + Pb collisions the values are

	T_i (GeV)
SPS	0.19
RHIC	0.22
LHC	0.25

The initial energy densities ε_i are higher than the nucleon energy density in nuclei by about an order of magnitude. We stated in sections 1 and 2 that for such energy densities (and temperatures) one should expect a transition of nuclear matter into quark-gluon plasma. However, the initial temperatures are not high enough for us to expect ideal QGP formation, at most we might hope for nonideal QGP.

In estimating the quantities ε_i and T_i we have used the ideal fluid approximation. Note that this approximation for quarks and gluons does not imply that interaction in the system is small. It is important that the interaction be properly taken into account by the equation of state $p = p(\varepsilon)$. Among the papers devoted to this topic we should mention Refs.[76—78]. It is well known that the ideal fluid approximation is applicable if the characteristic collision times and mean free paths of quarks, antiquarks and gluons in the system satisfy the conditions

$$\begin{aligned} \tau &\ll t \\ \lambda &\ll L \end{aligned} \quad , \tag{20}$$

where t and L are the time and scale factors over which such macroscopical hydrodynamic quantities as energy density and pressure change considerably. To what degree is this picture valid for ultrarelativistic ion-ion reactions? Since the characteristic mean free path of quarks $\lambda \simeq 1$ fm and the system dimension in the transverse direction $R_A \sim A^{1/3}$ fm, the second condition in Eq. (20) is more or less fulfilled. On the other hand, in realistic collisions $\tau \simeq t$, and it is necessary to consider the viscosity of the strongly interacting matter. This can be taken into account by adding to the right-hand side of the equation of motion $\partial_\mu T^{\mu\nu} = 0$, a term that accounts for energy dissipation under hydrodynamic expansion [22]. The effect of viscosity, as one would expect, is to decrease the initial energy density in heavy-ion collisions [22].

With the recent progress in the modelling of high energy nuclear collisions, the simple estimates in this section can be put on a more quantitative footing.

4. LEPTON PAIRS AND PHOTON PRODUCTION FROM QGP AND HADRONIC GAS

In the previous sections we presented theoretical considerations in favour of thermalized strongly interacting matter formation in ultrarelativistic heavy-ion collisions. In this section, we discuss dynamical processes in thermal matter and the experimental manifestations of these processes. The problems of hot nuclear matter diagnostics resemble in a sense those related to Big Bang synthesis: the initial conditions should ideally be reconstructed from data of

observational astronomy. Of particular importance is to find out which observed collision characteristics carry information on hot matter formation. By «hot matter», we mean either QGP or hadronic gas, depending on the relation between the initial temperature T_i and phase transition temperature T_c. (This line of reasoning assumes a first order phase transition).

Among the experimental QGP signals reported in the literature, we will single out the following:

a) Analyses of lepton, photon, J/ψ, φ, ρ, η, and η' spectra can be used to trace the properties of matter at its hottest stage.

b) Searches for primordial remnants in the observed hadronic features (discontinuities in the momentum distribution of the secondaries [14], particle ratios [11] and droplets of strange matter [15]).

The quark-gluon plasma is a macroscopic ensemble characterized by its temperature, its pressure and chemical composition (the number of different types of particles). It can exist in the process of nuclear collisions, however, in a restricted temperature interval $T_i > T_c$. When, under hydrodynamic expansion, the temperature falls below T_c, QGP is transformed into hadronic gas. As T drops below T_f, there occurs decay into free hadrons. One problem of QGP diagnostics is that soft processes of hadronization may substantially distort information on parton system evolution. Since the parton hadronization mechanism is still largely unknown, the results of decoding observed inclusive hadron spectra, as well as other hadron characteristics in search for QGP signals, are model-dependent and cannot serve as a rigorous proof of QGP existence.

The advantage of leptons and photons from the viewpoint of hot strongly interacting matter diagnostics is that they escape practically without secondary interactions. So, one can consider dilepton and photon spectra as a probe of the hottest stage of the reaction. There are many competing sources of dileptons and photons both before and after the hot stage of the collision. Reconstruction seems next to impossible. The best that one can do is to evaluate the contribution from each source to ascertain whether or not it is dominant in some part of phase space or if it has distinct properties that make separation feasible. We will proceed along these lines by considering four regions in the invariant mass M of the produced dileptons. For invariant mass M above the J/ψ peak, the spectrum is dominated by Drell-Yan production. The spectrum around $\simeq 1$ GeV is dominated by ρ, ω and φ decays. Dileptons with invariant masses in the region 1.5—3.0 GeV seem to be mostly derived from hadronic reactions with a possible contribution from quark annihilation. Again, this analysis assumes a thermalized initial state (except for Drell-Yan, of course). A nonequilibrium picture may yield results that are different.

The last region of invariant mass $M < m_\rho$, is a region of «soft» dilepton production. There are many sources of dileptons with masses $M < m_\rho$: π^0 and η Dalitz decays, $\pi^+\pi^-$ annihilation (for $M^{e^+e^-} > 2m_\pi$), pion scattering with virtual bremsstrahlung, and if quark-gluon plasma is formed, there will be quark-antiquark annihilation and quark-quark (antiquark, gluon) scattering with virtual bremsstrahlung.

As for photons, one can expect the transverse momentum spectrum in the region $p_\perp \sim 3$—5 GeV to be dominated by hard QCD compton processes. For $p_\perp \simeq 3$ GeV, π^0 and η decays are important as well as bremsstrahlung from binary collisions within the thermal medium. We will consider these mechanism in this and the following sections.

We consider dilepton and photon emission first from an ideal QGP (without interactions) followed by an ideal hadronic gas. In section 2 we stressed that in heavy-ion collisions the real situation is complicated by interactions among the QGP and hadronic plasma constituents. We will delay discussions of the effects of such complications on dilepton and photon spectra until the next section.

4.1. Annihilation Reactions. Consider in greater detail dilepton production by a thermalized medium. Such a medium can be either quarks, antiquarks and gluons in a deconfined phase or it can be an hadronic gas. For the sake of simplicity and to illustrate the theoretical approach, we shall assume that the hadronic sector in the confined phase consists solely of pions. The validity of this will be explored quantitatively later. In first order perturbation theory dilepton production is described by the diagram of Fig.9, where «a» is a pion or a quark. In quantum electrodynamics e^+e^- annihilation is similar to that shown in Fig.9. The cross section for the process $e^+e^- \to \mu^+\mu^-$ is of the form

$$\sigma(M) = \frac{4\pi}{3} \frac{\alpha^2}{M^2} \left(1 + \frac{2m^2}{M^2} \right)\left(1 - \frac{4m^2}{M^2} \right)^{1/2}, \qquad (21)$$

where α is the fine structure constant, m is the muon mass and M is the mass of virtual photon γ^*. In the case of quark and antiquark annihilation, one must include a multiplicative colour factor $N_c = 3$ in Eq.(21). Another deviation from Eq.(21) as applied to quarks is that it must reflect their fractional electric charge $e_u = 2/3$, $e_d = -1/3$. Then the l^+l^- pair production cross section by quark-antiquark annihilation is given by

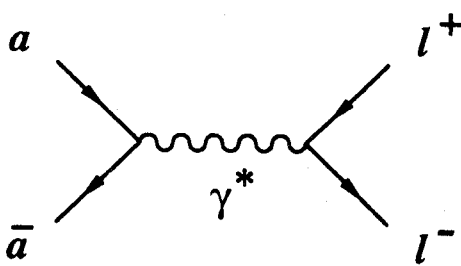$$\sigma_q(M) = F_q \, \sigma(M), \qquad (22)$$

Fig.9. Dilepton production by quark-antiquark (or two-pion) annihilation

where $E_q = 4N_c \sum_f e_f^2$ and the summation is carried out over the quark flavours. In this expression we have also averaged over the spins of the quarks in the initial state. Equations (21) and (22) require some modification if particles a and $\bar{a}$ are pions. Since pions are colourless and spinless particles with unit electric charge, the factor of averaging over spin and colour gives unity. It is necessary to multiply Eq.(22) by a form factor $|F_\pi(M)|^2$ [79]. The cross section for the process $\pi^+\pi^- \to l^+l^-$ is rather simply written

$$\sigma_\pi(M) = |F_\pi(M)|^2 \, \sigma(M) \left(1 - \frac{4m_\pi^2}{M^2}\right)^{1/2}. \tag{23}$$

To calculate the rate of dilepton production per unit time per unit volume from thermalized matter, one averages the annihilation cross section $\sigma(a\bar{a} \to l^+l^-)$ over the momentum distribution functions of primary particles and antiparticles

$$R(a\bar{a} \to l^+l^-) = \int \frac{d^3P}{(2\pi)^3} f(P) \int \frac{d^3\bar{P}}{(2\pi)^3} \bar{f}(\bar{P}) \, \sigma(a\bar{a} \to l^+l^-) \, \upsilon_{rel}, \tag{24}$$

where υ_{rel} is the relative velocity of the primary particle and antiparticle,

$$\upsilon_{rel} = \frac{\sqrt{(E\bar{E} - P\bar{P})^2 - m_a^4}}{E\bar{E}}, \tag{25}$$

and E, P ($\bar{E},\bar{P}$) are the energy and momentum of the particles (antiparticles). Note here the following important point: the above formalism is in fact more general than the current would tend to suggest. If the background matter is out of equilibrium and the momentum distribution functions are known, they can be used in Eq.(24). In what follows we will be concerned with the case $T \geq m_a$, then we may approximate the distributions by

$$f(p) \simeq \exp(-E/T). \tag{26}$$

In this case the integration of the expression Eq.(24) gives

$$\frac{dN}{d^4x dM^2 \pi dp_\perp^2 dy^*} = \frac{\sigma_a}{(2\pi)^5}\left(1 - \frac{4m_a^2}{M^2}\right)\exp\left(-E^*/T\right) \qquad (27)$$

for the number of lepton pairs with invariant mass M, emitted from the element d^4x of 4-volume of thermalized nuclear matter. In Eq.(27), $p_\perp$ is the transverse momentum of the dilepton, y^* and E^* are the rapidity and energy of the dilepton in the rest frame of element of nuclear matter, respectively. But one knows that

$$E^* = M_\perp \cosh y^*, \qquad (28)$$

where

$$M_\perp = \sqrt{M^2 + p_\perp^2} \qquad (29)$$

is the transverse mass of the dilepton.

Equation (27) solves the first part of the problem, i.e., quantifies a lepton pair generation rate in the rest frame of the element of thermalized nuclear matter. The second part is to sum this rate over the evolution of the nuclear matter as it undergoes hydrodynamic expansion (Fig.8). Consider dilepton production from QGP, which exists at $\tau_i < \tau < \tau_Q$. Under one-dimensional hydrodynamic expansion, integration of eq.(27) over $d^4x = \pi R_A^2 d\chi \tau\, d\tau$ leads to

$$\frac{d\sigma}{dM^2 dy\, d^2p_\perp} = \frac{\sigma_q \pi R_A^2}{(2\pi)^5} \int_{\tau_i}^{\tau_Q} \tau\, d\tau \int_{-Y_m}^{+Y_m} d\chi \exp\left(\frac{-M_\perp \cosh(y-\chi)}{T}\right). \qquad (30)$$

Here, y is the dilepton rapidity in the CMS of the AA collision and $y = y^* + \chi$. In setting the integration limits, the scaling conditions as well as the lifetimes of the QGP phase are taken into account. For $y \ll Y_m$ ($y \simeq 0$ is the central region), integration over χ gives

$$\int d\chi \exp\left(-\frac{M_\perp \cosh \chi}{T}\right) \simeq 2K_0\left(\frac{M_\perp}{T}\right) \simeq \left(\frac{2\pi T}{M_\perp}\right)^{1/2} \exp\left(-\frac{M_\perp}{T}\right). \qquad (31)$$

According to the scaling solution (Eqs.7—12), there is a one-to-one mapping between proper time and temperature $\tau T^3 = \tau_i T_i^3$. Therefore, $\tau d\tau = T_i^6 \tau_i^2 3dT/T^7$ and we write [80,22,81]

$$\frac{d\sigma}{dM^2 \, dy \, d^2 p_\perp} = \frac{\sigma_q}{(2\pi)^5} \pi R_A^2 \, 3T_i^6 \, \tau_i^2 \int_{T_c}^{T_i} \frac{dT}{T^7} \left(\frac{2\pi T}{M_\perp}\right)^{1/2} \exp\left(-\frac{M_\perp}{T}\right). \quad (32)$$

Formulas for the contribution to dilepton production from the pion gas can be obtained in a similar manner [22] by replacing $T_c \to T_i$, $T_c \to T_f$, and $\sigma_q \to \sigma_\pi$. We concentrate on central collisions of equally massed nuclei.

The next problem is how to estimate dilepton production from the mixed phase? One way to estimate this contribution is to consider the mixed phase as a simple mix of QGP and hadronic gas at a temperature T_c [22]. As long as the volume fraction f of the quark-qluon phase is specified (as a function of time) formulas for dilepton emission from QGP and hadronic gas can be used to estimate the contribution from the mixed phase. The entropy density is $S(f,T_c) = S_q(T_c)f + S_h(T_c)(1-f)$, where $S_q = 148aT^3$, $S_\pi = 12aT^3$ and $a = \pi^2/90$. Similar expressions can be written for the energy density. In the mixed phase the entropy density decreases, not by decreasing T but by converting quark-gluon plasma to hadron matter at lower entropy density. The fraction $f(t)$ can be expressed as

$$f(t) = \frac{1}{r-1}\left[r\frac{t_1}{t} - 1\right], \quad (33)$$

where $\tau = 37/3$ is the ratio of the number of degrees of freedom in the two phases and t_1 is the time of mixed phase formation.

Another simple approach to mixed and hadronic phases was developed in Ref.[82]. The change in T throughout the entire hadron phase is not very large $(T_f \approx T_c)$. Therefore, the contribution from the mixed and hadron phases may be parametrized to be $\alpha \exp(-E/T_c)$. If QGP is formed, its presence should manifest itself by a nonexponential torus [82—84]. For dilepton spectra, one gets [82]

$$\frac{dN}{dM^2 dy \, d^2 p_\perp} = \frac{\alpha^2}{12\pi^4} \frac{(R_A + R_B)^2}{\pi R_A^2 R_B^2} \left[\frac{c}{4a_q} \frac{dN^{AB \to \pi}}{dy}\right]^2 \times$$

$$\times \int d\chi \left\{ \int_{T_c}^{T_i} \frac{3dT}{T^7} \exp\left[-\frac{M_\perp \cosh(y-\chi)}{T_c} \right] + \right.$$

$$\left. + \frac{\lambda}{T_c^6} \exp\left[-\frac{M_\perp \cosh(y-\chi)}{T_c} \right] \right\}, \tag{34}$$

where $c = 3.6$, $a_q = 5.25$ and $\lambda = 125$. Typically this idealized Maxwell construction for two-phase equilibrium is invoked as a model of the hadronization process in fluid dynamical approaches. However, it is by no means clear that the QCD nucleation rate is large enough for this idealization to be anywhere near reality. In Ref.[85] the nucleation rate is computed for a first order phase transition using a set of rate equations to study the time evolution of expanding quark-gluon plasma as it converts into hadronic matter. The authors calculated the fraction of space occupied by hadronic matter as a function of time and obtained a time delay when compared to the adiabatic Maxwell idealization. The temperature had to drop about 20 % below T_c before nucleation and bubble growth was strong enough to cause reheating. The difference in dilepton yield between an idealized Maxwell construction of phase coexistence and a dynamical phase transition with finite nucleation and phase conversion rates has been investigated in Ref.[86]. It is difficult to say *a priori*, whether the «supercooling» scenario would enhance or suppress the dilepton yield because there are competing effects. On the one hand, there is a tendency to suppress the yield because the temperature is below T_c during the phase transition, and lower temperature immediately implies a lower dilepton yield. On the other hand, there is an enhancement in the yield because the transition lasts about 30 fm/c with a Maxwell construction, while the finite phase conversion rates cause a delay of the completion of the transition by about 11 fm/c, implying a longer time period for dilepton production. The combined effect gives an enhancement of dilepton yield by a factor 2 near the ρ-peak. It would seem very useful to perform an experiment which would be able to measure the dilepton mass spectra at $M \sim 600$ MeV to better than a factor 2. Within the context of present experiments, this is probably not feasible.

We have discussed the «canonical» Bjorken model for strongly interacting matter evolution. The hadrons do not interact after «freeze-out» in this model. There is no rigorous way to uniquely define the temperature at freeze-out, T_f. Since T_f is a phenomenological parameter, one should check the sensitivity of dilepton yield to the numerical value chosen. The dilepton yield will increase as the chosen value of the parameter T_f is lowered. But even after the passage to

free-streaming has occured, hadron trajectories may occasionally overlap, leading to *hh* reactions which produce additional lepton pairs [87,88]. If T_f is lowered, the thermal contribution is increased, but the free-streaming contribution is reduced. Such competition leaves the total dilepton mass spectrum rather insensitive to the choice of freeze-out temperature T_f.

The formula for the quark-antiquark annihilation cross section was represented above in the Born approximation. The question of how QCD corrections can change the tree level results was discussed in Refs.[89,90] and [91]. A rich structure of the propagation modes inside the plasma were discovered [92], which resulted in a huge enhancement in the dilepton production rate over the Born annihilation term. However, these calculations were performed for the lepton pairs at rest in the plasma rest frame, and did not allow for phenomenological analyses in arbitrary kinematical regions. The corrections are essential for low massed pairs ($M \leq T$) and are negligible for large masses ($M \geq 1$ GeV). The corrections to the dilepton emission rate from a QGP in kinematical configurations $M^{e^+e^-} \leq T$ and $q_\perp^{e^+e^-} \gg T$ were calculated in Ref.[93]. The ratio between the first and zeroth order QCD corrections $\sim (4\pi/3\alpha_s)\,(T^2/M^2)\ln(ET/m_q^2)$ (m_q is the thermal mass quark) and reaches $\sim 10^2 - 10^3$ for $M \simeq 0.02$ GeV, $M_\perp \simeq 1$ GeV, and $T = 300$ MeV.

4.2. Bremsstrahlung. The fundamental principle that drives bremsstrahlung is simply that when charged particles are accelerated there may be accompanying emission of real or virtual quanta. Particles in collision clearly undergo accelerations and are therefore prone to this phenomenon. In hadron-hadron or nucleus-nucleus collisions there are several reaction possibilities depending upon the available energy. At low energies proton-neutron bremsstrahlung contributes the most. At intermediate energies pions are produced reasonably frequently and they might collide with a nucleon or possibly another pion, charged or uncharged. At much higher energies since the system is comprised mainly of thermal or nearly thermal pions, pion-pion bremsstrahlung is the dominant contributor. And if conditions allow QGP formation, the QCD constituents scatter and are therefore also prone to the same physical phenomenon.

In colliding nuclear systems where the densities rise to several times normal nuclear matter density, radiation is complicated by the fact that binary collisions are no longer free from multiple-collision interference effects. Specifically, if the mean time between collisions becomes small enough to be comparable to the time it takes radiation to properly materialize, then total radiation is no longer just the sum of independent binary reactions but rather a complicated coherent sum of many. Since high-mass dileptons originate from processes on

very short time scales and low-mass pairs from those with longer times, it stands to reason that the low-mass pairs will suffer from this effect to a larger extent. The net result of such interference, referred to as the Landau-Pomeranchuk (LP) effect [94], is to suppress production of low-mass dileptons, at least for some very dense system. First principles calculations valid in all kinematical regions for the real or virtual photons including the LP effect are computationally difficult, especially when they include most of what is known about the strong interaction. A proper treatment requires complete knowledge of the dynamics. Estimates of these phenomena have been done in some limiting cases.

Low energy calculations using a one-boson-exchange (OBE) model for the strong interaction were reported in Refs. [95] and [96]. Here the bremsstrahlung cross sections were calculated gauge invariantly including both external and internal radiation using the OBE model while fitting the coupling constants and form factors to the proton-neutron elastic cross sections over a fairly wide energy range. A less ambitious but much cheaper way to get the cross sections is to use a soft-photon approximation [97,25,98]. Contributions having radiation originating from the internal lines in the diagrams are neglected while radiation from external lines is computed. The propagator leading to the external lines of the diagrams develops a singularity as the energy of the photon approaches zero, making these diagrams clearly dominant as compared with all others. Neglecting the others is valid as long as $q_0 \tau < 1$ in nonrelativistic, and $q_0 \tau << \gamma^2$ in relativistic collisions, where $q_0 = |\vec{q}|$ is the energy of the photon, τ is the duration of the strong-interaction collision and γ is the usual Lorentz factor. Precisely how good the approximation is for semi-hard or for lepton pairs with finite invariant mass is not clear. Therefore, the soft-photon approximation has been compared with results from a Born approximation calculation [99]. At dilepton invariant mass ~100 MeV the soft-photon approximation was found to be surprisingly good. The scope of this section of our review includes bremsstrahlung estimations using the soft-photon methos with LP interference discussed briefly.

Low's theorem [100] in its true form established an equivalence in the sructure of the $q_0 \to 0$ bremsstrahlung matrix elements independent of whether the radiating particles are hadrons or leptons, whether they carry spin or not and independent of any differences that exist between their interactions. It is useful since it means that in this limit no matter how complicated the diagrams or how computationally difficult the interaction becomes, the matrix element separates into its on-shell counterpart times a multiplicative factor describing the electrodynamics of the reaction. The radiated quanta might not satisfy the Einstein condition $q^2 = 0$ but instead appear as a massive (virtual) photon. Extrapolation
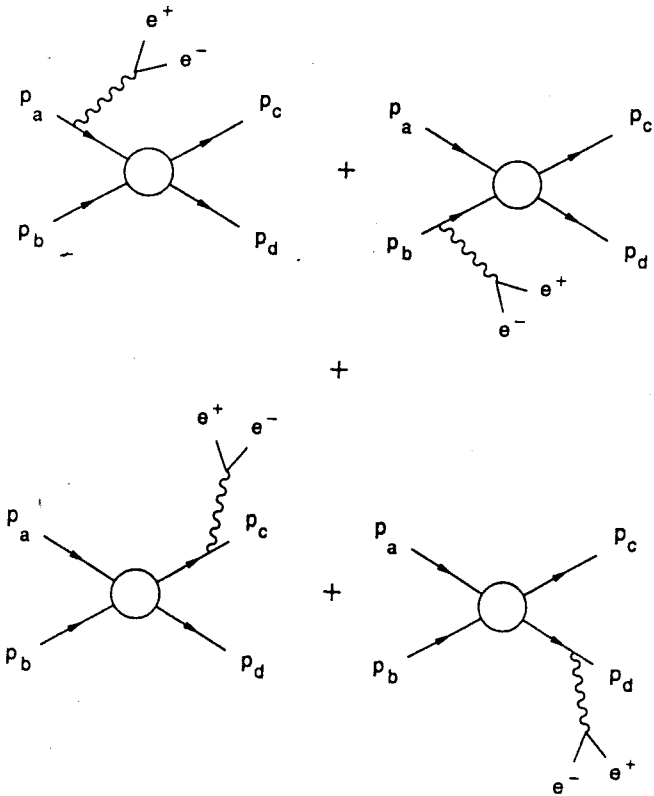
Fig.10. Virtual bremsstrahlung in the soft-photon approximation includes radiation from external lines only. Shown here is a completely general scattering process which might include nucleons, pions or quarks and gluons

from real photon production to electron-positron pairs is done consistently by inserting a four-momentum conserving delta function at the photon-dilepton vertex. Any differences in the matrix element due to the finite mass of the virtual photon are ignored. The diagrams for the elementary process $a + b \rightarrow$ $\rightarrow c + d + l^+ + l^-$ are shown in Fig.10 where the reaction partners might be nucleons or nucleon resonances, mesons, or even quarks or antiquarks and gluons. The discussion is completely general at this point. Then the differential cross section is reduced to the quasi-elastic scattering cross section and at the same time to the production of an e^+e^- pair through decay of a virtual photon [97,25,98,101]

$$\frac{d\sigma^{e^+ e^-}_{ab \to cd}}{dM^2} = \frac{\alpha^2}{8\pi^4} \frac{1}{M^2} \int |\varepsilon \cdot J|^2_{ab \to cd} \frac{d\sigma_{ab \to cd}}{dt} \delta(M^2 - q^2)$$

$$\times \delta^4(q - (p_+ + p_-)) \, d^4q \, \frac{d^3p_+ \, d^3p_-}{E_+ E_-} \, dt, \tag{35}$$

where t is the four-momentum transfer in the $a + b \to c + d$ collision, M is the invariant mass of the $e^+ e^-$ pair, p_+ and p_- are the momenta of the positron and electron respectively, and

$$|\varepsilon \cdot J|^2 = \sum_\delta \varepsilon_\delta \cdot J \varepsilon_\delta \cdot J. \tag{36}$$

The sum is taken over all photon polarizations, and the current J in the reaction $a + b \to c + d$ is

$$J^\mu = -Q_a \frac{p_a^\mu}{p_a \cdot q} - Q_b \frac{p_b^\mu}{p_b \cdot q} + Q_c \frac{p_c^\mu}{p_c \cdot q} + Q_d \frac{p_d^\mu}{p_d \cdot q}, \tag{37}$$

where the Q_i s are particle charges in units of the proton charge.

For very general scattering processes subject only to over charge conservation the polarization summed (and angle-averaged) electrodynamic factor is [101]

$$|\varepsilon \cdot J|^2_{ab \to cd} = \frac{1}{q_0^2} \{ -(Q_a^2 + Q_b^2 + Q_c^2 + Q_d^2) - 2Q_a Q_b \, \mathcal{F}(\vec{\beta_a^*}, \vec{\beta_b^*}) +$$

$$+ 2Q_a Q_c \, \mathcal{F}(\vec{\beta_a^*}, \vec{\beta_c^*}) + 2Q_a Q_d \, \mathcal{F}(\vec{\beta_a^*}, \vec{\beta_d^*}) + 2Q_b Q_c \, \mathcal{F}(\vec{\beta_b^*}, \vec{\beta_c^*}) +$$

$$+ 2Q_b Q_d \, \mathcal{F}(\vec{\beta_b^*}, \vec{\beta_c^*}) - 2Q_c Q_d \, \mathcal{F}(\vec{\beta_c^*}, \vec{\beta_c^*}) \}, \tag{38}$$

where the function

$$\mathcal{F}(\vec{x}, \vec{y}) = \frac{(1 - \vec{x} \cdot \vec{y})}{2\sqrt{(1 - \vec{x} \cdot \vec{y})^2 - (1 - x^2)(1 - y^2)}} \times$$

$$\times \left\{ \ln \left| \frac{\vec{x} \cdot \vec{y} - x^2 - \sqrt{(1 - \vec{x} \cdot \vec{y})^2 - (1 - x^2)(1 - y^2)}}{\vec{x} \cdot \vec{y} - x^2 + \sqrt{(1 - \vec{x} \cdot \vec{y})^2 - (1 - x^2)(1 - y^2)}} \right| + \right.$$

$$\left. + \ln \left| \frac{\vec{x} \cdot \vec{y} - y^2 - \sqrt{(1 - \vec{x} \cdot \vec{y})^2 - (1 - x^2)(1 - y^2)}}{\vec{x} \cdot \vec{y} - y^2 + \sqrt{1 - \vec{x} \cdot \vec{y})^2 - (1 - x^2)(1 - y^2)}} \right| \right\}, \tag{39}$$

the CM velocities'inner products can be related to invariants through

$$\vec{\beta_a^*} \cdot \vec{\beta_b^*} = \frac{-\lambda(s, m_a^2, m_b^2)}{(s + m_a^2 - m_b^2)(s - m_a^2 + m_b^2)}$$

$$\vec{\beta_a^*} \cdot \vec{\beta_c^*} = \frac{2s(t - m_a^2 - m_c^2)}{(s + m_a^2 - m_b^2)(s + m_c^2 - m_d^2)} + 1$$

$$\vec{\beta_a^*} \cdot \vec{\beta_d^*} = \frac{-2s(t - m_a^2 - m_c^2)}{(s - m_a^2 - m_b^2)(s - m_c^2 + m_d^2)} - \frac{s + m_c^2 - m_d^2}{s - m_c^2 + m_d^2}$$

$$\vec{\beta_b^*} \cdot \vec{\beta_c^*} = \frac{-2s(t - m_a^2 - m_c^2)}{(s - m_a^2 + m_b^2)(s + m_c^2 - m_d^2)} - \frac{s + m_a^2 - m_b^2}{s - m_a^2 + m_b^2}$$

$$\vec{\beta_b^*} \cdot \vec{\beta_d^*} = \frac{2s(t - m_a^2 - m_c^2)}{(s - m_a^2 + m_b^2)(s - m_c^2 + m_d^2)} + \frac{(s + m_a^2 - m_b^2)(s + m_c^2 - m_d^2)}{(s - m_a^2 + m_b^2)(s - m_c^2 + m_d^2)}$$

$$\vec{\beta_c^*} \cdot \vec{\beta_d^*} = \frac{-\lambda(s, m_c^2, m_d^2)}{(s + m_c^2 - m_d^2)(s - m_c^2 + m_d^2)} \tag{40}$$

and

$$(\beta_a^*)^2 = \frac{\lambda(s, m_a^2, m_b^2)}{(s + m_a^2 - m_b^2)^2}, \qquad (\beta_b^*)^2 = \frac{\lambda(s, m_a^2, m_b^2)}{(s - m_a^2 + m_b^2)^2}$$

$$(\beta_c^*)^2 = \frac{\lambda(s, m_c^2, m_d^2)}{(s + m_c^2 - m_d^2)^2}, \qquad (\beta_d^*)^2 = \frac{\lambda(s, m_c^2, m_d^2)}{(s - m_c^2 + m_d^2)^2}. \tag{41}$$

The kinematic function $\lambda(x, y, z) = x^2 - 2(y + z)x + (y - z)^2$ [102] and $s \geq \max\{(m_a + m_b)^2, (m_c + m_d)^2\}$. Equation (38) is very powerful since it is valid for any masses. For instance, it can be applied to reactions such as $q + g \to q + g + \gamma^* \to q + g + l^+ + l^-$ or even $g + g \to q + \bar{q} + \gamma^* \to q + \bar{q} + + l^+ + l^-$.

For equal-mass scattering as in pion-pion or quark-quark (or antiquark) $m_a = m_d = m_c = m_d = m$, and Eq. (38) reduces to

$$
\begin{aligned}
|\varepsilon \cdot J|^2_{ab \to cd} = \frac{1}{q_0^2} \Big\{ & -(Q_a^2 + Q_b^2 + Q_c^2 + Q_d^2) - \\
& - 2(Q_a Q_b + Q_c Q_d) \frac{s - 2m^2}{\sqrt{s(s - 4m^2)}} \ln\left(\frac{\sqrt{s} + \sqrt{s - 4m^2}}{\sqrt{s} - \sqrt{s - 4m^2}} \right) + \\
& + 2(Q_a Q_d + Q_b Q_c) \frac{s - 2m^2 + t}{\sqrt{s + t - 4m^2}(s + t)} \ln\left(\frac{\sqrt{s + t} + \sqrt{s + t - 4m^2}}{\sqrt{s + t} - \sqrt{s + t - 4m^2}} \right) + \\
& + 2(Q_a Q_c + Q_b Q_d) \frac{2m^2 - t}{\sqrt{t(t - 4m^2)}} \ln\left(\frac{\sqrt{4m^2 - t} + \sqrt{-t}}{\sqrt{4m^2 - t} - \sqrt{-t}} \right) \Big\},
\end{aligned}
\tag{42}
$$

where $s \geq 4m^2$ and $-(s - 4m^2) \leq t \leq 0$. This expression is still very useful since it is valid for any momentum transfer and any energy. However, it is somewhat lengthy so a simpler yet approximate description would be convenient. If charge is conserved along each of the lines ($Q_a = Q_c$ and $Q_b = Q_d$) and if the momentum transfer is relatively small ($|t| < 4m^2$), then a good approximation for the equal-mass electrodynamic factor is [103]

$$
|\varepsilon \cdot J|^2_{ab \to cd} \simeq \frac{2}{3} \frac{1}{q_0^2} \left(\frac{-t}{m^2} \right) \left[(Q_a^2 + Q_b^a) - \frac{3}{2} Q_a Q_b f(s) \right],
\tag{43}
$$

where

$$
\begin{aligned}
f(s) = & \frac{s}{2(s - 4m^2)} - \frac{(s - 4m^2)}{2s} - \frac{m^2}{s} \left\{ \frac{2\sqrt{s}}{\sqrt{s - 4m^2}} + \left(\frac{\sqrt{s}}{\sqrt{s - 4m^2}} \right)^3 + \right. \\
& \left. + \frac{\sqrt{s - 4m^2}}{\sqrt{s}} \right\} \ln\left(\frac{\sqrt{s} + \sqrt{s - 4m^2}}{\sqrt{s} - \sqrt{s - 4m^2}} \right).
\end{aligned}
\tag{44}
$$

The interference function behaves as follows. In the limit $\sqrt{s}/m \to 2$, $f(s) \to -2/3$ and as $\sqrt{s}/m \to \infty$, $f(s) \to 0$. Eqs. (43) and (44) are extremely useful because the result is linear in t. This approximation is quite good as long as particles are at least as massive as pions. For processes involving lighter particles, one must resort to Eq. (42). Finally note that if one of the

incoming particles is electrically neutral as in $\pi^{\pm}\pi^0$, Eq. (43) reduces to the much used expression [25]

$$|\varepsilon \cdot J|^2 \simeq \frac{2}{3} \frac{1}{q_0^2} \left(\frac{-t}{m^2} \right).$$ (45)

The common $1/q_0^2$ dependence in all of these electrodynamic factors allows analytic integration over the virtual photon and lepton momenta when inserted into Eq. (35). The resulting mass spectrum is

$$\frac{d\sigma^{e^+e^-}_{ab \to cd}}{dM^2} = \frac{\alpha^2}{4\pi^2} \frac{\hat{\sigma}(s)}{M^2} \times$$

$$\times \left\{ \ln \left(\frac{(\sqrt{s} - (m_a + m_b)) + \sqrt{(\sqrt{s} - (m_a + m_b))^2 - M^2}}{(\sqrt{s} - (m_a + m_b)) - \sqrt{(\sqrt{s} - (m_a + m_b))^2 - M^2}} \right) - \right.$$

$$\left. - \frac{2\sqrt{(\sqrt{s} - (m_a + m_b))^2 - M^2}}{(\sqrt{s} - (m_a + m_b))} \right\},$$ (46)

where

$$\hat{\sigma}(s) \equiv \int_{t^-}^{t^+} dt \, (q_0^2 |\varepsilon \cdot J|^2_{ab \to cd}) \frac{d\sigma_{ab \to cd}}{dt}$$ (47)

for which the momentum-transfer limits are $t^{\pm} = m_a^2 + m_c^2 - 1/2s \{(s + m_a^2 - m_b^2)(s + m_c^2 - m_d^2) \mp \lambda^{1/2}(s, m_a^2, m_b^2) \lambda^{1/2}(s, m_c^2, m_d^2)\}$. For reactions with two distinct masses $m_a = m_c = m_1$ and $m_b = m_d = m_2$, these limits reduce to $t^- = -\lambda^{1/2}(s, m_c^2, m_d^2)/s$ and $t^+ = 0$. And finally, for equal-mass scattering the limits reduce further to $t^- = -(s - 4m^2)$ and $t^+ = 0$.

Evaluation of the e^+e^- production cross section proceeding along these lines neglects the momentum of the virtual photon in the phase-space δ-function. Strictly speaking, one should correct for this by including the multiplicative factor

$$\frac{R_2(s_2, m_a^2, m_b^2)}{R_2(s, m_a^2, m_b^2)} = \frac{\lambda^{1/2}(s_2, m_a^2, m_b^2)}{\lambda^{1/2}(s, m_a^2, m_b^2)} \frac{s}{s_2}$$ (48)

(with $s_2 = s + M^2 - 2\sqrt{s}\, q_0$) before integrating Eq. (35) [104].

Having the elementary bremsstrahlung cross sections which are exact in the limit $q_0 \to 0$, one can employ the independent particle approximation from kinetic theory to write the number of reactions per unit time per unit volume, i.e., the rate, as

$$\frac{dN_{ab}^{e^+e^-}}{d^4xdM^2} = g_{ab} \int ds \int \frac{d^3p_a}{(2\pi)^3} \int \frac{d^3p_b}{(2\pi)^3} e^{-\beta(E_a + E_b)} \times$$

$$\times \frac{d\sigma_{ab}^{e^+e^-}}{dM^2} v_{rel} \delta(s - (p_a + p_b)^2), \qquad (49)$$

where

$$v_{rel} = \frac{\sqrt{(p_a \cdot p_b)^2 - m_a^2 m_b^2}}{E_a E_b},$$

β is the inverse temperature and $q_{ab} = (2s_a + 1)(2s_b + 1) N_c^a N_c^b$ is the spin and colour degeneracy. Integrating over both particles' momenta yields

$$\frac{dN_{ab \to cd}^{e^+e^-}}{d^4xdM^2} = \frac{T^6 q_{ab}}{16\pi^4} \int_{z_{min}}^{\infty} dz \frac{\lambda(z^2T^2, m_a^2, m_b^2)}{T^4} \mathcal{K}_1(z) \frac{d\sigma_{ab \to cd}^{e^+e^-}}{dM^2}(z) \qquad (50)$$

where $z_{min} = (m_a + m_b + M)/T$, $z = \sqrt{s}/T$, and $\mathcal{K}_1$ is a modified Bessel function. But keep in mind that $s \geq \max\{(m_a + m_b)^2, (m_c + m_d)^2\}$. Note that for pion-pion bremsstrahlung this reduces to the form used in Ref. [22]. Elastic scattering cross sections are all that is needed in order to calculate the rate of electron-positron production through virtual bremsstrahlung from pion-pion processes, quark-quark or quark-gluon processes, etc.

Observed distributions are obtained only after integration of the production rates over likely scenarios for the history of the colliding nuclear system. Using assumptions detailed in section 3 regarding evolution, the pure quark and hadronic phase contributions can be calculated [22] with

$$\frac{dN}{dy\,dM} = 3\pi R_A^2 T_i^6 \tau_i^2 \int_{T_c}^{T_i} \frac{dT}{T^7} \frac{dN^q}{d^4xdM}, \qquad (51)$$

and

$$\frac{dN}{dy\,dM} = 3\pi R_A^2 T_i^6 \, \tau_i^2 r^2 \int\limits_{T_f}^{T_s} \frac{dT}{T^7} \frac{dN^\pi}{d^4 x dM}, \tag{52}$$

while the mixed phase contribution from quark and pion processes are

$$\frac{dN_{mixed}^q}{dy\,dM} = \frac{\pi R_A^2}{2} \left(\frac{T_i}{T_c}\right)^6 \tau_i^2 (r-1) \frac{dN^q}{d^4 x dM} \, (T = T_c), \tag{53}$$

and

$$\frac{dN_{mixed}^\pi}{dy\,dM} = \frac{\pi R_A^2}{2} \left(\frac{T_i}{T_c}\right)^6 \tau_i^2 \, r(r-1) \frac{dN^\pi}{d^4 x dM} \, (T = T_c). \tag{54}$$

Here r denotes the ratio of the number of degrees of freedom of the QGP constituents to that of the hadron gas constituents ($r \simeq 12$). Input to these formulas are simply the elastic scattering cross sections.

4.2.1 *Pions.* Attention is restricted to charge-neutral and charge-anticharge pion scattering since the cross sections and electrodynamics suppress the other isospin channels. With the approximate electrodynamic factor, Eq. (35) becomes

$$\frac{d\sigma_{\pi\pi}^{e^+ e^-}}{dM^2} = \frac{\alpha^2}{6\pi^2} \frac{\overline{\sigma}_{\pi\pi}(s)}{M^2} \Phi(\sqrt{s}, m_\pi, M) \left\{\frac{4}{3} + \frac{1}{2} f(s)\right\}, \tag{55}$$

where $\sigma_{\pi\pi} \sim \sigma_{\pi^+\pi^0} + \sigma_{\pi^-\pi^0} + \sigma_{\pi^+\pi^-}$, the momentum transfer weighted cross section is $\overline{\sigma}(s)$, and the function

$$\Phi(\sqrt{s}, m_\pi, M) = \ln\left(\frac{(\sqrt{s} - 2m_\pi) + \sqrt{(\sqrt{s} - 2m_\pi)^2 - M^2}}{\sqrt{s} - 2m_\pi - \sqrt{(\sqrt{s} - 2m_\pi)^2 - M^2}}\right) -$$
$$- \frac{2\sqrt{(\sqrt{s} - 2m_\pi)^2 - M^2}}{(\sqrt{s} - 2m_\pi)}. \tag{56}$$

If $d\sigma/dt$ is a symmetric function of t and u, then

$$\overline{\sigma}(s) = 2\sigma_{el}(s) \left[\frac{s}{4m_\pi^2} - 1\right]. \tag{57}$$

The elastic pion-pion cross section can be parametrized in the following way:
 a) For $\sqrt{s} \leq 0.6$ GeV the chiral model expression is used [105,106],

$$\sigma_{el}(s) = \frac{2}{3} \frac{1}{F_\pi^4} \frac{1}{16\pi} s \left[1 - \frac{5m_\pi^2}{s} + \frac{7m_\pi^4}{s^2} \right] \qquad (58)$$

with the pion decay constant $F_\pi = 0.098$ GeV;

 b) At the collision energy near the rho mass, $0.6 < \sqrt{s} \leq 1.5$ GeV, the largest contribution to the $\pi\pi$-scattering amplitude is due to resonance formation. Therefore,

$$\sigma_{el}(s) = \frac{g_{\rho\pi\pi}^4}{48\pi s} \frac{(s - 4m_\pi^2)^2}{(s - m_\rho^2)^2 + m_\rho^2 \Gamma_\rho^2}, \qquad (59)$$

where the coupling constant $g_{\rho\pi\pi} \simeq 6$, $m_\rho = 0.775$ GeV, and $\Gamma_\rho = 0.155$ GeV;

 c) For large collision energy $\sqrt{s} > 1.5$ GeV, σ_{el} becomes energy independent $\sigma_{el} \simeq 5$ mb.

Equations (50) and (55) provide a good approximation for the rate of e^+e^- production from the sum of $\pi^+\pi^0$, $\pi^-\pi^0$ and $\pi^+\pi^-$ processes.

From the point of view of principles, a more complete estimate for this production rate would include an angular description for pion-pion elastic scattering instead of merely the integrated result. Then the exact electrodynamic factor could be properly folded in each scattering process which clearly matches the real situation more closely. The exact electrodynamic factor is given by Eq. (42) with Q_a, Q_b, Q_c, $Q_d = 0$, ± 1 and $m_a = m_b = m_\pi$. In a recent study of pion-pion bremsstrahlung [101], a field theory calculation was done using σ, ρ, and $f(1270)$ meson-exchange to model the strong interaction. The quantum numbers for these exchanged particles are ($I = 0$, $J = 0$), ($I = 1$, $J = 1$), and ($I = 0$, $J = 2$), respectively. An effective Lagrangian of

$$\mathcal{L}_{int} = g_\sigma \sigma \partial_\mu \vec{\pi} \cdot \partial^\mu \vec{\pi} + g_\rho \vec{\rho^\mu} \cdot (\vec{\pi} \times \partial_\mu \vec{\pi}) + g_f f_{\mu\nu} \partial^\mu \vec{\pi} \cdot \partial^\nu \vec{\pi} \qquad (60)$$

was used. The authors illustrated the method by showing details of the calculation of $\sigma(\pi^+\pi^- \to \pi^+\pi^-)$. The differential cross section is proportional to the square of the matrix element describing the overlap of initial and final two-hadron states. In this model, six terms comprise the matrix element: t and s channel σ-, ρ- and f-exchange processes. Since mesons are composites,

modification at short distances or high momentum transfers was included. Momentum-transfer damping monopole form factors were inserted at the vertices of t-channel diagrams. Their form was

$$h_\alpha(t) = \frac{m_\alpha^2 - m_\pi^2}{m_\alpha^2 - t},$$

(61)

where m_α was either the σ, ρ, or the f mass depending upon which meson was exchanged.

In this model finite resonance lifetimes were incorporated into the scalar, vector, and tensor boson propagators. For instance, the f propagator used was

$$i\,\mathcal{P}^{\mu\nu\alpha\beta} = \frac{-i\left\{\frac{1}{2}\left(\frac{1}{3}g^{\mu\nu}g^{\alpha\beta} - g^{\mu\alpha}g^{\nu\beta} - g^{\mu\beta}g^{\nu\alpha}\right)\right\}}{k^2 - m_f^2 + im_f\Gamma_f}.$$

(62)

The matrix element was written

$$\mathcal{M} = \mathcal{M}_1 + \mathcal{M}_2 + \mathcal{M}_3 + \mathcal{M}_4 + \mathcal{M}_5 + \mathcal{M}_6,$$

(63)

where

$$\mathcal{M}_1 = \frac{-g_\sigma^2 h_\sigma^2(t)(2m_\pi^2 - t)^2}{t - m_\sigma^2 + im_\sigma\Gamma_\sigma}, \qquad \mathcal{M}_2 = \frac{-g_\sigma^2(s - 2m_\pi^2)^2}{s - m_\sigma^2 + im_\sigma\Gamma_\sigma}$$

$$\mathcal{M}_3 = \frac{-g_\rho^2 h_\rho^2(t)(s - u)}{t - m_\rho^2 + im_\rho\Gamma_\rho}, \qquad \mathcal{M}_4 = \frac{g_\rho^2(u - t)}{s - m_\rho^2 + im_\rho\Gamma_\rho}$$

$$\mathcal{M}_5 = \frac{g_f^2\, h_f^2(t)}{t - m_f^2 + im_f\Gamma_f}\frac{1}{2}\left(\frac{1}{3}(2m_\pi^2 - t)^2 - (s - 2m_\pi^2)^2 - (2m_\pi^2 - u)^2\right)$$

$$\mathcal{M}_6 = \frac{g_f^2}{s - m_f^2 + im_f\Gamma_f}\frac{1}{2}\left(\frac{1}{3}(s - 2m_\pi^2)^2 - (2m_\pi^2 - t)^2 - (2m_\pi^2 - u)^2\right).$$

(64)
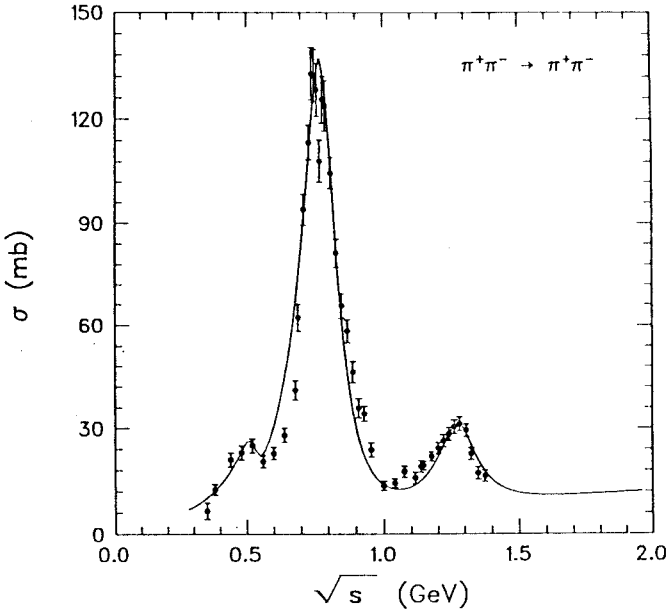
Fig.11. Elastic $\pi^+\pi^-$ cross section calculation as compared with experiment

Notice that as written g_σ and g_f are not dimensionless but $g_\sigma m_\sigma$ and $g_f m_f$ are. In pion-pion scattering, the elastic differential cross section is

$$\frac{d\sigma}{dt} = \frac{|\mathcal{M}|^2}{16\pi s(s - 4m_\pi^2)}. \tag{65}$$

Within this model for the matrix element, $d\sigma/dt$ has qualitatively the right behaviour as compared with what is observed experimentally: for energies just below the ρ resonance the angular distribution is forwardly peaked, for $\sqrt{s}$ near m_ρ, the distribution becomes forward-backward symmetric, and finally above the resonance it is backward dominated. The numerical values for the coupling constants and widths were adjusted to $g_\sigma m_\sigma = 1.85$, $m_\sigma = 0.525$ GeV, $\Gamma_\sigma = 0.100$ GeV, $g_\rho = 6.15$, $m_\rho = 0.775$ GeV, $\Gamma_\rho = 0.155$ GeV, $g_f m_f = 7.2$, $m_f = 1.274$ GeV and $\Gamma_f = 0.176$ GeV. We show the results of the integrated cross section in Fig.11. Superb agreement with experiment was obtained for the energies shown. Other $\pi\pi$ processes ($\pi^\pm\pi^0 \rightarrow \pi^\pm\pi^0$) were calculated analogously. With all three cross sections, one can compute the rate
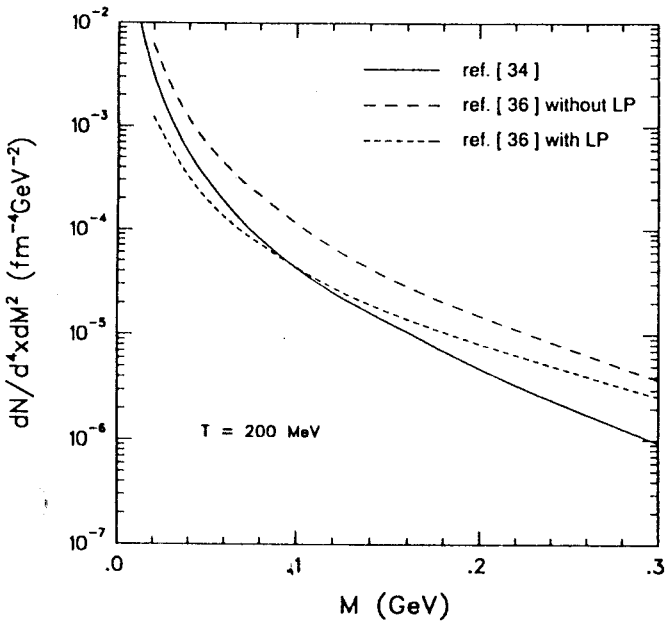
Fig.12. Dielectron mass spectrum from pion-pion bremsstrahlung using the full formalism (solid curve) as compared with approximate formulas with and without the Landau–Pomeranchuk effect

of pair production using Eqs. (46) and (47), which is exact within the soft photon approximation. The net result of using the more exact formulas is a suppression as compared with the approximate result by a mere factor ~2.

Dielectrons with masses $\lesssim 100$ MeV are produced in $\pi\pi$ scattering at any kinematically allowed $\sqrt{s}$ and are therefore dominated near the ρ-peak; whereas higher mass pairs ($M \approx 300$ MeV) are effectively produced through $\pi\pi$ scattering with $\sqrt{s} \gtrsim m_\rho$. When $M \approx 300$ MeV in Eqs. (46) and (50) with $\sqrt{s}$ near the kinematically determined minimum (just below the ρ-peak) the production rate is strongly suppressed by the logarithm and radical. The soft photon approximation is less reliable for high masses but this suggests that it is imperative to have a reasonably accurate calculation of the cross section for $\sqrt{s} > m_\rho$. Such calculations would be incomplete if they excluded the tensor $f(1270)$ meson.

An approach somewhat different from this one has been taken by Cleymans et al. in Ref. [107], where within a soft-photon approximation the LP effect is included in pion-pion bremsstrahlung estimates. The starting formulas are quite different since multiple-collision interferences are included. We show in Fig.12 the LP-corrected (and LP-uncorrected) results and compare it with the
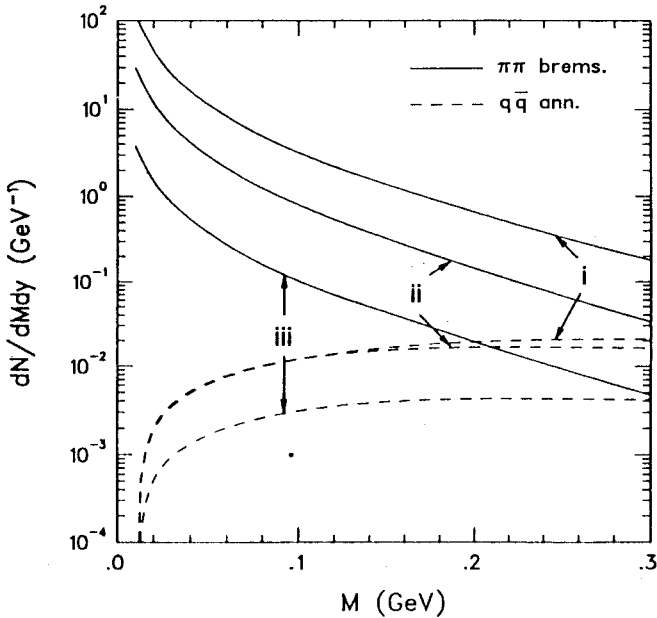
Fig.13. The low-mass dielectron yields from pion-pion bremsstrahlung (solid curves) and quark-antiquark annihilation (dashed curves) in the Born approximation. The three scenarios are (i) $T_i = 300$, $T_c = 200$, and $T_f = 140$ MeV, and (ii) $T_i = 250$, $T_c = 150$, and $T_f = 100$ MeV and finally, (iii) correspond to $T_i = 200$, $T_c = 150$, and $T_f = 140$ MeV

calculation by Haglin et al. from Ref. [101]. Several points are worth mentioning here. Firstly, the low-mass dielectron production rate is suppressed by the LP effect in a dense pion gas by nearly an order of magnitude. Secondly, the two curves without LP effect represent two different approximations for hadronic bremsstrahlung. The results from Cleymans et al. were calculated by approximating production with charge-neutral pion scattering. In the bremsstrahlung cross section the electrodynamics were approximated by a simple expression that allowed use of simply the total elastic pion cross section — which was parametrized. The results are quite close to the more detailed calculation from Haglin et al., where other processes were included and the electrodynamics were properly handled for each reaction. Also, phase space corrections in the latter calculation introduce a slightly different mass dependence in the results. While the LP effect is indeed important, one sees that its effect is at the level of uncertainty in the approximated elementary bremsstrahlung cross sections.

And it should therefore be considered equally important as the effects from including all the pion-pion processes, calculated as accurately as possible.

As discussed above, integration over the mixed and cooling phases for the pions gives the estimated total yield. We show it in Fig.13 for three different collections of initial, critical and final temperatures. The results from quark-antiquark annihilation discussed previously are also presented.

4.2.2. *Quarks and Gluons.* Quark scattering processes introduce additional difficulties due to their fractional charge, their colour, and their possibility for elastic scattering with their own force mediating bosons, the gluons. But the formalism from Ref. [101] is capable of handling the general case. The diagrams from Fig.10 are again the relevant ones to be evaluated. This time the charged external lines are u or d quarks (or antiquarks) and neutral external lines are gluons. The calculation reported in Ref. [101] included six distinct quark-quark (or antiquark) and four quark-gluon (or antiquark) reactions. Those with equal-charge scattering were neglected. Other processes like $q\bar{q} \to gg$ and its reverse process were shown to give a rather small contribution to the low-mass e^+e^- production rate so they were also neglected. The approximate expression for $|\varepsilon \cdot J|^2$ cannot be applied to current quarks since the range of validity is too small ($t < 4m_q^2 \approx 1.0 \times 10^{-4}$ GeV^2); so one resorts to Eq. (42). By setting the mass to m_q and by setting Q_a and Q_b to the appropriate quark electric charges, one has the exact electrodynamic factor in these reactions. When considering quark (or antiquark)-gluon processes, Eq.(38) must be used with $m_a = m_q$ and $m_b = 0$.

The strong interaction differential cross sections $d\sigma_{qq}/dt$ and $d\sigma_{qg}/dt$ are well known in the perturbative vacuum at the one-gluon-exchange level to be [108]

$$\frac{d\sigma_{ab}}{dt} = \frac{C_{ab}\, 2\pi\alpha_s^2}{t^2}, \tag{66}$$

where

$$C_{ab} = \begin{cases} 1 & (qg \to qg) \\ \dfrac{4}{9} & (qq \to qq) \end{cases}. \tag{67}$$

For hot hadronic matter this is clearly inadequate. Consider the dominant t-channel gluon exchange amplitude for the diagram in Fig.14. $\mathcal{M}^{ab} = \alpha_s \Gamma_\mu^a \mathcal{D}^{\mu\nu} \Gamma_\nu^b$, where $\mathcal{D}^{\mu\nu} = g^{\mu\nu}/t$ is the gluon propagator and $\Gamma_{\mu,\nu}^{a,b}$ are vertex functions for particles a, b. It is obvious that $\mathcal{M}^{ab}$ is singular in the

Fig.14. *t*-channel gluon-exchange diagram

q q

Γ_μ^a

$q\,(g)$ Γ_ν^b $q\,(g)$
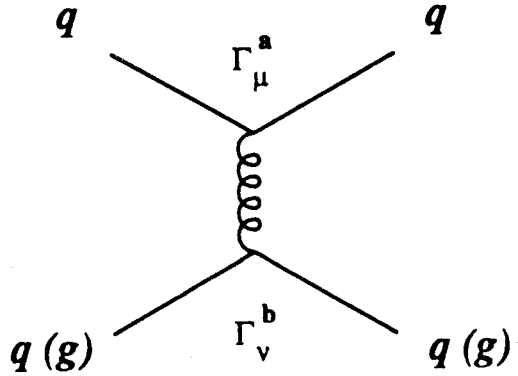
zero momentum-transfer limit. But at finite temperatures static colour-electric fields are shielded by quarks and gluons in the plasma, and colour-magnetic fields are also shielded by non-perturbative effects [109]. Colour-electric shielding modifies the $\mu = \nu = 0$ components of $\mathcal{D}^{\mu\nu}$ in such a way that

$$\mathcal{M}_E^{ab} \simeq \alpha_s(t)\,\Gamma_0^a\,\mathcal{D}^{00}\,\Gamma_0^b \simeq \frac{\alpha_E(t)}{t}\,\Gamma_0^a\Gamma_0^b, \tag{68}$$

where the running coupling constant [109]

$$\frac{\alpha_E(t)}{t} = \frac{\alpha_s(t)}{t - m_E^2}, \tag{69}$$

and the colour-electric mass $m_E^2 = 6\pi\alpha_s T^2$. The medium-modified magnetic scattering amplitude can be written

$$\mathcal{M}_M^{ab} \simeq \alpha_s(t)\,\Gamma_i^a\,\mathcal{D}^{ij}\,\Gamma_j^b \simeq -\frac{\alpha_M(t)}{t}\,\Gamma_i^a\Gamma_i^b, \tag{70}$$

where the effective magnetic coupling $\alpha_M(t)/t = \alpha_s(t)/(t - m_M^2)$ and the colour-magnetic mass $m_M^2 = c\,\alpha_s^2 T^2$. Lattice gauge calculations [110] give $c \simeq 20$—30. In the small t limit the vertex functions reduce to $\Gamma_\mu^a \simeq p_\mu^a$, where

p_μ^a is the momentum of particle a. Averaging over colour and spin degrees of freedom gives the differential cross section [109]

$$\frac{d\sigma_{ab}}{dt} = C_{ab} \frac{8\pi}{s^2 t^2} [\alpha_E(t) \, p_0^a \, p_0^b - \alpha_M(t) \, \vec{p}^{\,a} \cdot \vec{p}^{\,b}]^2, \tag{71}$$

where $s = (p_a + p_b)^2$.

Unfortunately, $d\sigma_{ab}/dt$ depends on the quark-quark (gluon) orientation in the scattering through $\vec{p}_a \cdot \vec{p}_b$. For arbitrary orientation of vectors $\vec{p}_a$, $\vec{p}_b$ one cannot obtain a closed expression for $d\sigma^{ab}/dt$, but if vector $\vec{p}_a$ is antiparallel to $\vec{p}_b$, $d\sigma_{ab}/dt$ reduces to

$$\frac{d\sigma^{ab}}{dt} = C_{ab} \frac{\pi}{2} \frac{\alpha_s^2(t)(2t - m_E^2 - m_M^2)^2}{(t - m_E^2)^2 (t - m_M^2)^2}. \tag{72}$$

Note that this expression is exact for massless quark (antiquark) scattering. For $T \sim 200—300$ MeV, $\alpha_s \simeq 0.2—0.3$, $m_E \simeq 2.2T$ and $m_M \simeq 1.5T$. If one assumes that the colour-electric mass is roughly equal to the colour-magnetic mass, $m_E \simeq m_M$, then the m_q dependence can be restored in the differential cross sections

$$\frac{d\sigma^{qg}}{dt} = \frac{2\pi\alpha_s^2(t)}{s^2(t - m_E^2)^2} (s - m_q^2)^2 \tag{73}$$

$$\frac{d\sigma^{qq}}{dt} = \frac{4}{9} \frac{2\pi\alpha_s^2(t)}{s^2(t - m_E^2)^2} (s - 2m_q^2)^2. \tag{74}$$

Using these expressions there is no sizeable change in the dilepton production rates or final spectra. So instead one can safely use Eq.(72). Note that in the limit m_E, $m_M \to 0$ (free space), it reproduces Eq.(66) for the perturbative vacuum.

Putting together Eqs. (35), (42), (50) and (72), one has the rate of e^+e^- production from all the quark (antiquark)-gluon or quark (antiquark)-quark processes. In Fig. 15 we show results of the sum of $qq(\bar{q}\bar{q})$ and $qg(\bar{q}g)$ scat-
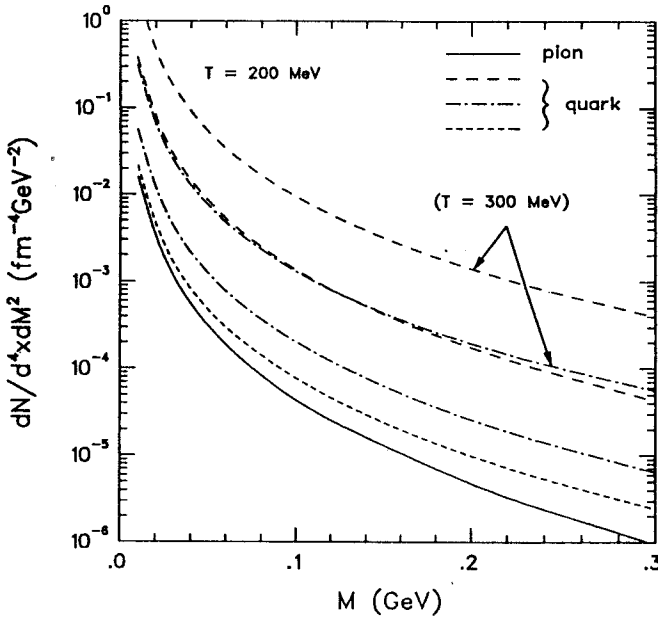
Fig.15. Dielectron production rate from quark and gluon processes

tering with virtual bremsstrahlung at temperatures $T = 200$ and 300 MeV. Three quark curves are shown: current quarks with mass 5 MeV, «medium» quarks with temperature-dependent mass $[2\pi\alpha_s(T)/3]^{1/2}T$, where $\alpha_s(T) = 6\pi/[(33 - 2N_f)\ln(aT/T_c)]$ and $a \sim 8$, and finally, «constituent» quarks with mass 300 MeV. Since the quark mass dependence in the production rate for small masses is roughly $\ln(1/m_q)$ due to Eq.(42) and the temperature dependence is roughly T^6, an upper limit on the rate is one that uses $m_q = 5$ MeV at $T = 300$ MeV. Similarly, a lower limit on the rate is one that uses $m_q = 300$ MeV at the phase transition temperature. Based on the results of Fig.15 where a quark and pion comparison is facilitated, one may conclude that at $T = 200$ MeV the (soft) virtual photon emissivities from competing medium quark versus pionic processes in the mass region $M \leq 2m_\pi$ differ by less than a factor of 4. In a different energy regime Kapusta et al. [111] reached the same conclusion while comparing real (energetic) photon emissivities of the QGP to that of hadronic
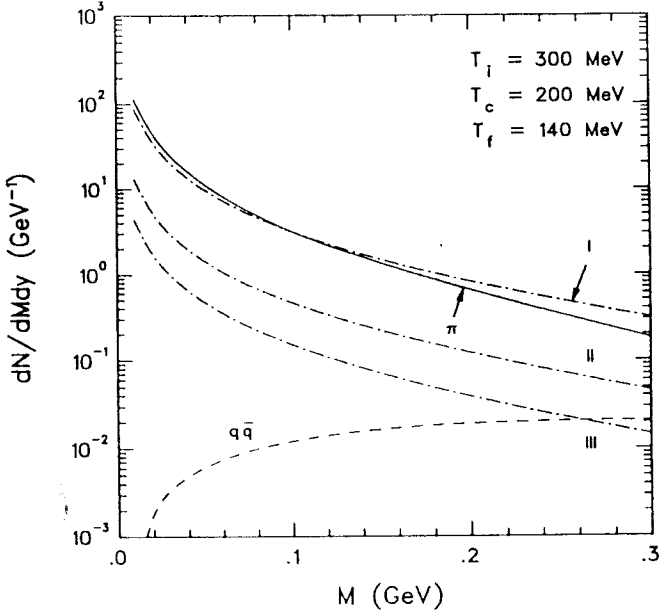
Fig.16. Dielectron yields using $T_i = 300$, $T_c = 200$ and $T_f = 140$ MeV

matter. This equal-luminous property appears also in the annihilation channels $q\bar{q} \to e^+e^-$ versus $\pi^+\pi^- \to \rho \to e^+e^-$ but only after an (invariant mass) integrated total emissivity. In particular, the emissivities $dN^{e^+e^-}/d^4x$ at $T = 200$ MeV for pions, medium quarks, and constituent quarks are approximately $\simeq 2.5$, 1.2 and $\simeq 1.1 (\times 10^{-9}$ GeV$^4)$, respectively.

In Fig.16 yields are shown. Invariant mass spectra from virtual bremsstrahlung of quarks and pions using relevant temperatures $T_i = 300$, $T_c = 200$ and $T_f = 140$ MeV are shown. For this collection of temperatures the pion cooling phase contribution is the larger contributor to its final spectrum, whereas the mixed phase dominates the resulting quark driven spectrum. The yield from $q\bar{q} \to \gamma^* \to e^+e^-$ annihilation in the Born approximation [22,106]. Throughout most of the range of dilepton invariant mass considered, the contribution from pion scattering with virtual bremsstrahlung are two or three orders of magnitude above the $q\bar{q}$ annihilation spectrum. An advantage of this soft-photon approach
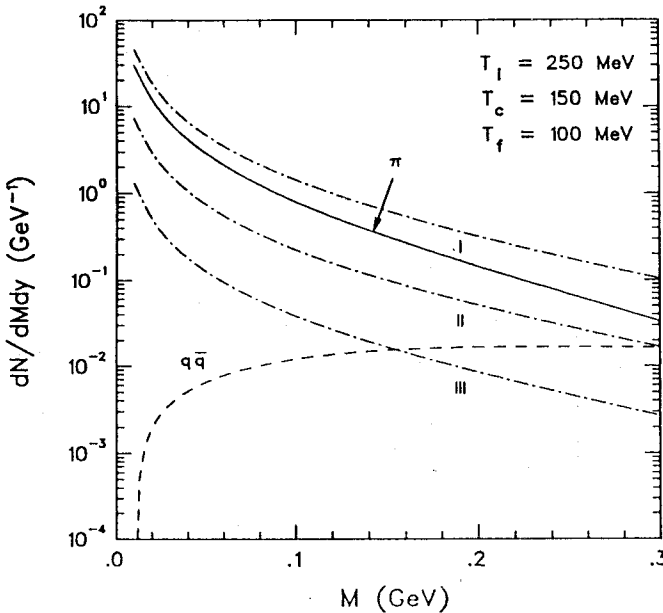
Fig.17. Dielectron yields using $T_i = 250$, $T_c = 150$ and $T_f = 100$ MeV

is that one could easily evaluate the bremsstrahlung contribution at finite $q_\perp$ or even impose some cuts in transverse momentum.

Another quite reasonable possibility for the relevant temperatures of the colliding system is $T_i = 250$, $T_c = 150$ and $T_f = 100$ MeV, corresponding to those used in Ref. [106] in a recent study of low-mass dilepton production. In Fig.17 we show results at these temperatures. Finally, for comparison purposes we show in Fig.18 still a different collection of temperatures having the lowest T_c which is compatible with lattice gauge theory data — $T_i = 200$, $T_c = 150$, and $T_f = 140$ MeV. As one can see from Figs. 17—18, the medium quark yield is always lower than the yields from pion scattering with bremsstrahlung. This being true, detection of quark degrees of freedom within this invariant mass region will be difficult in future heavy-ion experiments.

4.3 Single Photon Production. The same formalism can be applied to the calculation of single photon production from a QGP [82,84]. Direct photons from a QGP can arise from three processes: Compton scattering ($qg \to \gamma q$, $\bar{q}g \to \bar{q}\gamma$), annihilation processes ($q\bar{q} \to g\gamma$) and bremsstrahlung (with a quark
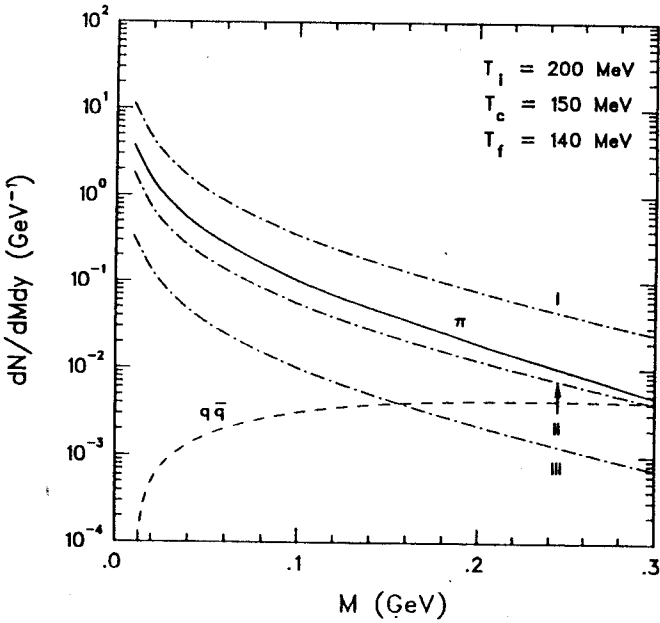
Fig.18. Dielectron yields using $T_i = 200$, $T_c = 150$ and $T_f = 140$ MeV

fragmenting into the photon), see Fig.19. The elementary cross sections for Compton and annihilation processes are [1,112,113]

$$\sigma(gq \rightarrow g\,\gamma) = \frac{16\pi\alpha\alpha_s}{81s} \ln\left(\frac{s}{4m_q^2}\right) \tag{75}$$
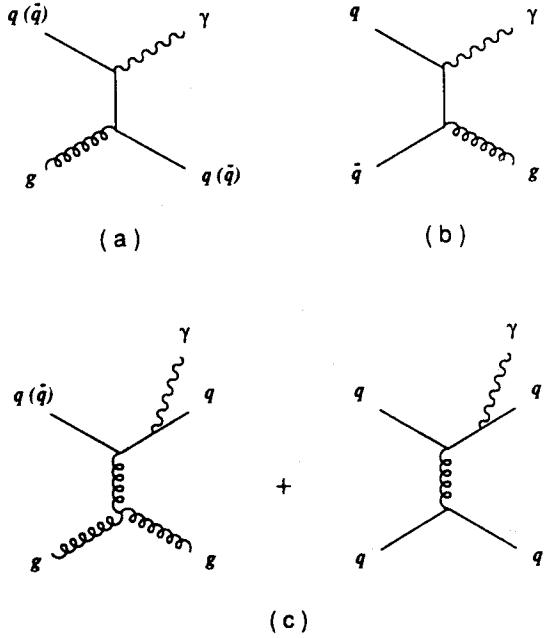
and

$$\sigma(q\bar{q} \rightarrow g\,\gamma) = \frac{4\pi\alpha\alpha_s}{3s} \ln\left(\frac{s}{4m_q^2}\right), \tag{76}$$

where s is the usual Mandelstam variable, m_q is the quark mass and α_s is the strong coupling constant. The production rate of single photons from a QGP was given in Ref. [113] as

$$\frac{d\sigma^\gamma}{d^4x} = \left\{\frac{\pi\alpha\alpha_s}{36} \ln\left(\frac{T}{m_{u,d}}\right) + \frac{\pi\alpha\alpha_s}{144} \ln\left(\frac{T}{m_s}\right)\right\} T^4. \tag{77}$$

Fig.19. Diagrams contributing to photon production: (a) Compton, (b) annihilation, (c) bremsstrahlung

(a)   (b)

(c)

As is well known [114], quark mass singularities may be screened by finite-temperature and finite-size effects. In this case

$$\frac{d\sigma^{\gamma}}{d^4x} \simeq \frac{5}{144} \ln\left(\frac{1}{\alpha_s}\right) T^4.$$

(78)

The integration over the similarity flow can be carried out exactly as before. The result for Compton plus annihilation diagrams is [82].

$$\frac{d\sigma}{dy\, d^2p_\perp} = \frac{\alpha\alpha_s}{p_\perp^4} \frac{4\sqrt{2\pi}\,\Gamma(3.5)}{\pi^4} \left[\frac{(R_A + R_B)^2}{R_A R_B}\frac{c}{4a_q}\frac{dN}{dy}\right]^2 \times$$

$$\times \ln\left(\frac{2}{\alpha_s}\right)\left\{P\left(3.5; \frac{p_\perp}{T_c}\right) - P\left(3.5; \frac{p_\perp}{T_i}\right)\right\}$$

(79)

where

$$P(3.5; a_c) - P(3.5; a_i) = \frac{1}{\Gamma(3.5)} \int_{a_i}^{a_c} t^{2.5} e^{-t} dt. \tag{80}$$

For the bremsstrahlung contribution, the 3.5 must be changed to 1.5 and the numerical factor in Eq. (79) is therefore, slightly different.

In Ref. [111], the thermal rate in the hadron phase has been computed to the same order as it was computed in the quark-gluon phase. The dominant reactions turned out to be the exact analogs of the QCD reactions, namely annihilation $\pi\pi \to \rho\gamma$ and Compton $\pi\rho \to \pi\gamma$ processes. In Ref. [111] the authors also estimated the contribution to the emission rate from the decay processes $\rho \to \pi^+\pi^-\gamma$ and $\omega \to \pi^0\gamma$. Other decays one may think of are too slow to contribute a significant amount to the thermal rate, although their contributions to the total yield in a high energy nucleus-nucleus collision may be non-negligible.

4.4. Proton Pair Production in Expanding Hot Hadronic Matter. The production of photon pairs from hadronic matter is mainly due to the elementary processes

$$q + \bar{q} \to 2\gamma, \tag{81}$$

in the QGP phase and

$$\pi^+ + \pi^- \to 2\gamma, \quad \pi^0 \to 2\gamma, \tag{82}$$

in the hadronic gas phase. The number of photon pairs emitted from the element of matter d^4x with invariant mass M, coming from the process in Eq. (81), is given by [115,116,117,118]

$$\frac{dN^{2\gamma}_{QGP}}{d^4xdM} = \frac{1}{(2\pi)^4} (M^2 - 4m_q^2)^{1/2} M^2 T^2 \sigma_{q\bar{q} \to \gamma\gamma}(M^2) \, G_+(T, M^2), \tag{83}$$

with

$$G_+(T, M^2) = \int_{m_q/T}^{\infty} dx(e^x + 1)^{-1} \times$$

$$\times \ln \left[\frac{1 + \exp\{-Wx + P[x^2 - (m_q/T)^2]^{1/2}\}}{1 + \exp\{-Wx - P[x^2 - (m_q/T)^2]^{1/2}\}} \right], \tag{84}$$

where

$$W = \frac{M^2}{2m_q^2} , \qquad (85)$$

and

$$P = \sqrt{W^2 - 1} . \qquad (86)$$

The quark-antiquark annihilation cross section $\sigma_{q\bar{q} \to \gamma\gamma}(M^2)$ in lowest order perturbation theory reads

$$\sigma_{q\bar{q} \to \gamma\gamma}(M^2) = 2\pi\alpha^2 N_c(2S + 1)^2 \sum_q \frac{e_q^4}{M^2 - 4m_q^2} \left\{ \left[1 + \frac{4m_q^2}{M^2} - \frac{8m_q^2}{M^2} \right] \times \right.$$

$$\left. \times \ln \left| \frac{M^2}{2m_q^2} \left(1 + \left[1 - \frac{4m_q^2}{M^2} \right]^{1/2} \right) - 1 \right| - \left(1 + \frac{4m_q^2}{M^2} \right)\left(1 - \frac{4m_q^2}{M^2} \right)^{1/2} \right\} ,$$

with $N_c = 3$, spin $S = 1/2$ and quark electric charges e_q. The production rate of photon pairs in the hadron gas has a structure similar to that of Eq. (83). The difference comes from the fact that the pions respect Bose instead of Fermi statistics. Instead of $G_+(T, M^2)$, one has

$$G_-(T, M^2) = \int_{m_\pi/T}^{\infty} dx(e^x - 1)^{-1} \times$$

$$\times \ln \left[\frac{1 - \exp \{-Wx - P(x^2 - (m_\pi/T)^2)^{1/2}\}}{1 - \exp \{-Wx + P(x^2 - (m_\pi/T)^2)^{1/2}\}} \right] , \qquad (87)$$

where

$$W = \frac{M^2}{2m_\pi^2} , \qquad (88)$$

and

$$P = \sqrt{W^2 - 1} . \qquad (89)$$

To lowest order in pertutbation theory the cross section is [117]

$$\sigma_{\pi^+\pi^- \to \gamma\gamma}(M^2) = \frac{4\pi\alpha^2}{s - 4m_\pi^2}\left[\left(\frac{1 + 4m_\pi^2}{M^2}\right)\left(\frac{1 - 4m_\pi^2}{M^2}\right)^{1/2} - \right.$$

$$\left. - 4m_\pi^2 M^2\left(1 - \frac{2m_\pi^2}{M^2}\right)\ln\left\{\frac{M^2}{2m_\pi^2}\left(1 + \left(1 - \frac{4m_\pi^2}{M^2}\right)^{1/2}\right) - 1\right\}\right].$$

There will also be an additional contributions from π^0 decay into two gammas [117,118]

$$\frac{dN^{\pi^0 \to \gamma\gamma}}{d^4x dM} = \Gamma_{\pi^0 \to \gamma\gamma}(M^2)\frac{M}{\pi^2}\delta(M^2 - m_{\pi^0}^2)\int_{m_{\pi^0}}^\infty dE\frac{E\sqrt{E^2 - m_{\pi^0}^2}}{\exp(E/T) - 1},$$

where $\Gamma_{\pi^0 \to \gamma\gamma} = \alpha^2 m_\pi^3/32\pi^3 f_\pi$, and the pion decay constant $f_\pi \simeq 0.98\, m_{\pi^0}^2$.

Using these formulas and integrating over the system evolution, one can obtain the contributions from QGP and hadronic phases to the diphoton invariant mass spectrum [118].

4.5. Properties of Dilepton Produced in QGP and Hadronic Gas. The formulas derived heretofore make it possible to calculate dilepton and photon spectra from a QGP and an hadronic gas. Now we consider several semi-quali-tative characteristics of the behaviour of these spectra, which may serve as thermalized nuclear matter diagnostics. We will discuss only the contributions from QGP and an hadronic gas; the background contributions to dilepton spectra will be discussed later.

Figures 20 and 21 show [22] the various contributions to the $\mu^+\mu^-$ invariant mass distribution $dN/dydM^2$ for two combinations of initial and critical tempe-ratures, T_i and T_c. Two-pion annihilation generally dominates quark-antiquark annihilation in the mass region $0.4 < M < 2.0$ GeV. This is due to the big peak in the pion form factor and to the relatively long time spent in the pion phase during evolution. The quark-phase contribution breaks through at approximately $M \simeq 2$ GeV due to the fact that quarks annihilate at a higher average tempe-rature than pions.

Recently the thermal production spectra have been calculated for LHC conditions [119]. The result is shown in Figs.22 and 23 for two different initial temperatures corresponding to $\varepsilon_i = 4.6$ GeV/fm^3, and approximately twice that
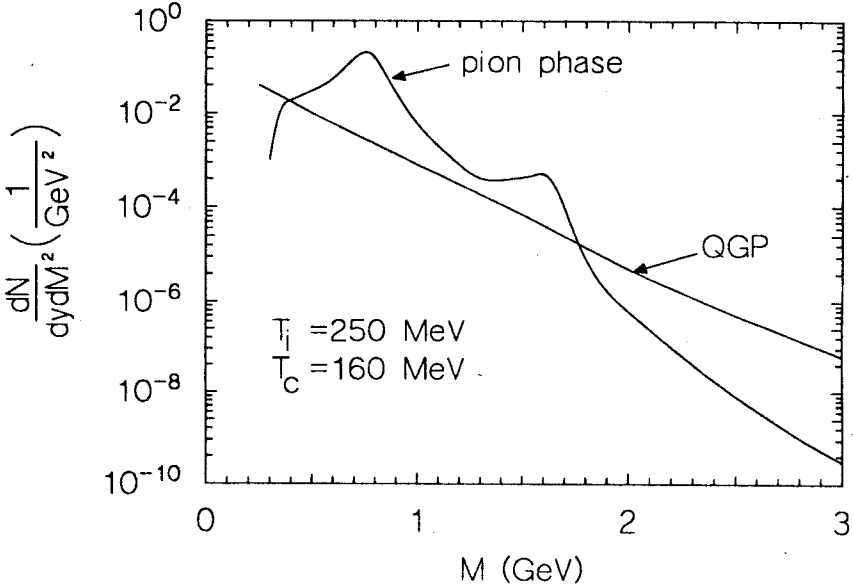
Fig.20. The dilepton mass distribution at central rapidities for Au + Au → μ⁺μ⁻X reactions with various combinations of initial and critical temperatures ($\tau_i = 1$ fm/c, $\pi R_A^2 = 127$ fm², and $T_f = 100$ MeV)

density. As we can see, the region of mass $M \lesssim 1.5—2.0$ GeV is dominated by emission from the hadronic gas. It is clear from Eqs. (32) and (34) that thermal emission time and dilepton mass are correlated. Pairs with largest mass ($M > M_\rho$) are produced at earliest times ($\tau \lesssim 1—0.1$ fm/c), when the temperature assumes its maximum value.

The hadronic dilepton production rates and yields have a peak around $M = m_\rho$ and go to zero at $M = 2m_\pi$. One can expect that the window $2m_e \leq \leq M \leq 2m_\pi$ is dominated by emission from the QGP. In the region of dilepton mass 300 MeV $\leq M \leq M_\rho$, the contribution from the QGP should show a prominent rise so that the full dilepton spectrum is expected to have a two-peaked structure [81.115]. Figure 24 shows the dilepton mass spectra for three different values of initial temperature as well as the origin of the two-peaked structure.
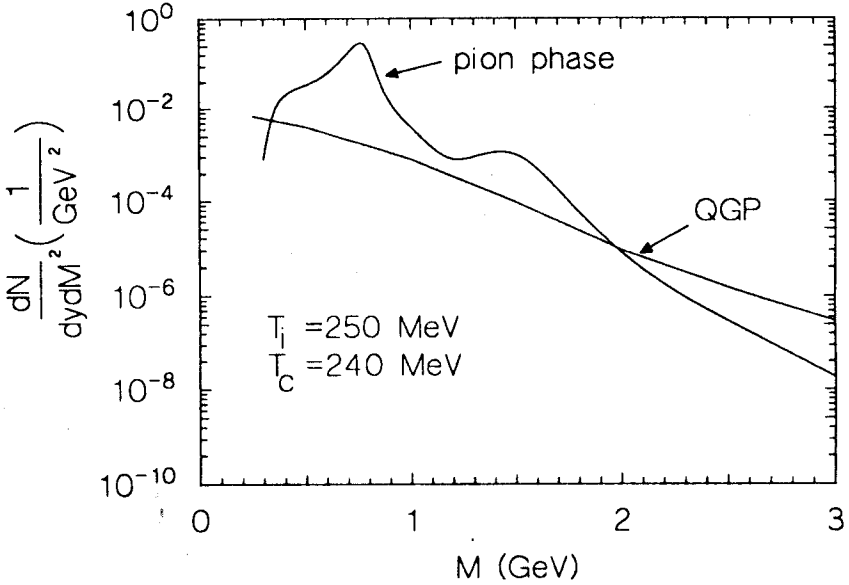
Fig.21. The dilepton mass distribution at central rapidities for $Au + Au \rightarrow \mu^+\mu^-X$ reactions with various combinations of initial and critical temperatures ($\tau_i = 1$ fm/c, $\pi R_A^2 = 127$ fm^2, and $T_f = 100$ MeV)

Equation (34) implies that the spectra of dileptons from QGP possesses an $M_\perp = [M^2 + p_\perp^2]^{1/2}$-scaling property, i.e., the spectra depend not separately on the variables M and $p_\perp$ but on their combination $M_\perp$. Omitting the mixed phase contribution for simplicity, we can express Eq. (34) as

$$\frac{dN}{dM^2 dy \, d^2 p_\perp} = \frac{\alpha^2}{12\pi^4} \left[\frac{e}{4a_q} \frac{dN^\pi}{dy} \right]^2 \frac{(R_A + R_B)^2}{\pi R_A^2 R_B^2} f(M_\perp, y),$$

where

$$f(M_\perp, y) = \int_{-Y}^{+Y} d\chi \left[\int_{T_c}^{T_i} \frac{3dT}{T^7} \exp\left\{ -\frac{M_\perp \cosh(y - \chi)}{T} \right\} \right].$$
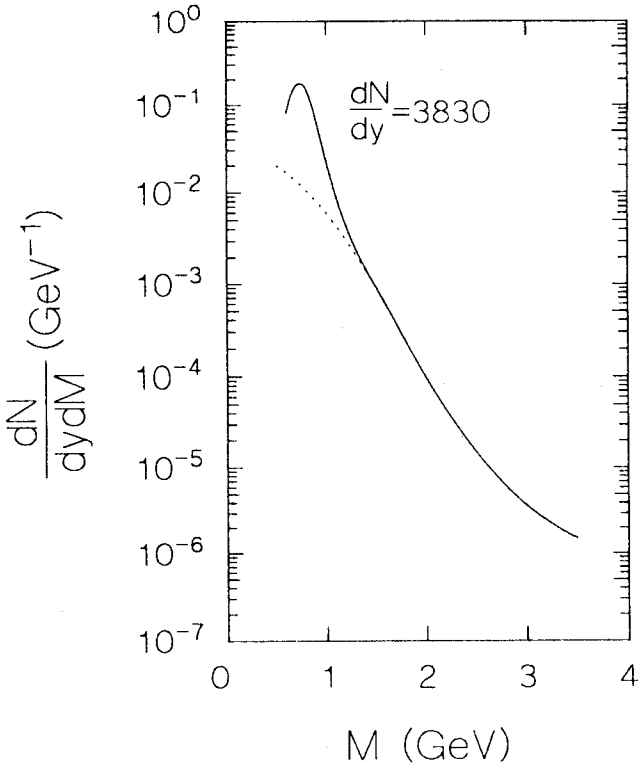
Fig.22. Production rate for thermal dileptons as a function of the dilepton mass M for LHC conditions for multiplicity $dN/dy = 1736$. Solid line is the pion phase contribution and the dotted line is the QGP contribution

So, the distribution of dilepton emission from QGP as a function of M for fixed values of $M_\perp$ and y must therefore be nearly constant. Indeed, Fig.25 (taken from Ref.[80]) shows that in the nonresonant region 1.2 GeV $<$ $< M <$ 2.7 GeV the dilepton production cross section at fixed $M_\perp$ is independent of M. But for the same variation on $M_\perp$, the absolute value of the differential cross section changes by several orders of magnitude! Similarly, the dilepton distribution over $p_\perp$ for fixed $M_\perp$ and y, must also be constant. On the other hand, the spectrum at fixed $M_\perp$ from hadronic plasma is not
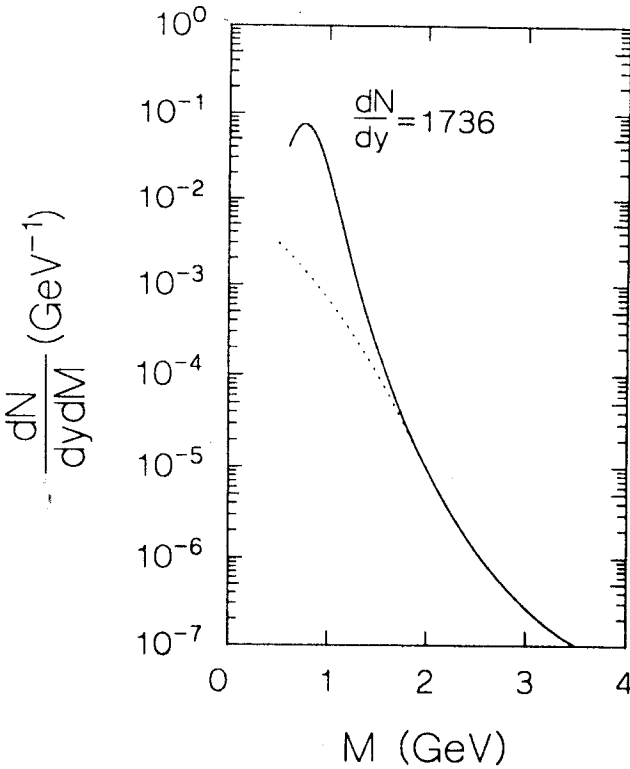
Fig.23. Same as Fig.22 but using a multiplicity $dN/dy = 3830$

constant due to the pion form factor. This fact may help in identification of dilepton production mechanisms in nuclear collisions. We shall discuss this more carefully in the following sections.

Up to now we considered only $\pi^+\pi^-$ annihilation as a source of dileptons from hadronic phase. But hadronic phase contains another particles, which take part in dilepton production [120]. As it was shown in [121], the production rates from reactions that involve axial-vector mesons dominate over contributions from all other reactions, when the dilepton invariant mass is above 1.5 GeV. Recently three-pion reactions in dilepton production from hadron gas have been investigated [122]. As one can expect, the three-pion processes amplify the ω and ϕ peaks in dilepton mass spectrum. The comparison of three-pion reactions with $\pi^+\pi^-$ annihilation shows that it is insufficient to consider only $\pi^+\pi^-$ annihi-
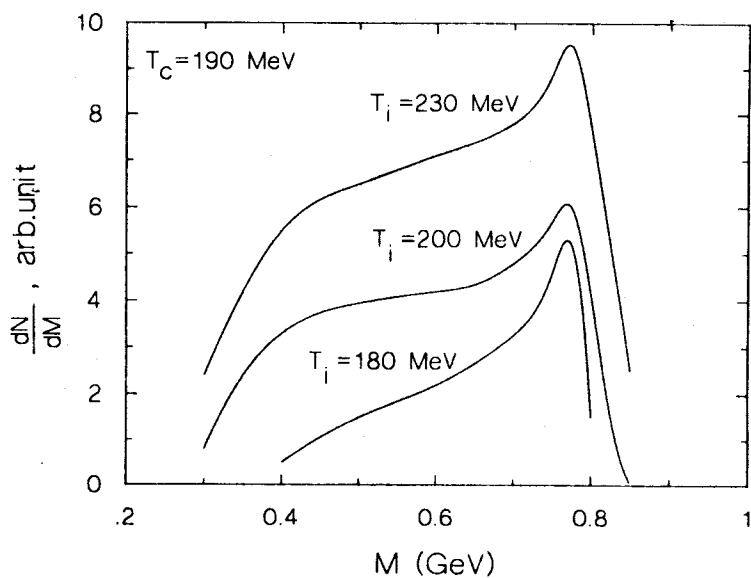
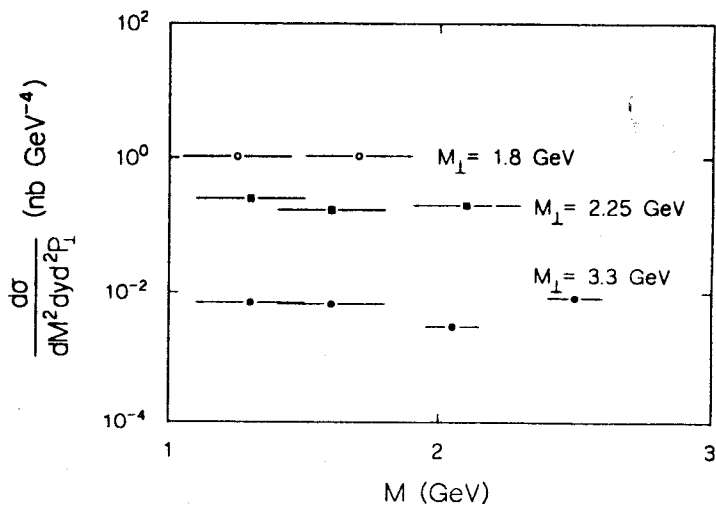**Fig.24. Two-peak** structure displayed

Fig.25. Dilepton production cross-section as a function of mass for three values of transverse mass. Dimuon spectrum is independent of mass if the transverse mass is fixed

lation when calculating dilepton production rate from a hadron gas in the continuum region above the ϕ peak.

4.6. Correlations in Dilepton Spectra. In the derivation of Eqs.(27) and (32), local thermodynamic equilibrium with an initial temperature T_i was assumed to be established in a system of quarks, antiquarks and gluons at a time τ_i. It should be stressed again that the fact of establishing any temperature in QCD is far from being obvious by itself. Indeed, the possibility of finding an associated temperature in the thermodynamical sense (or impossibility of introducing this characteristic) is not efficiently ascertained by QCD dynamics, known well only in the weak coupling region. At this stage, we think it is reasonable to try to solve the problem of thermalization experimentally. Since dileptons and photons are effectively emitted at times close to τ_i (contrary to hadrons), their spectra must be sensitive to the assumption of thermalization. In equilibrium QGP, dilepton production is mainly specified by the Boltzmann factor

$$\exp\left(-E^*/T_c\right) \simeq \exp\left[-(M^2 + P_\perp^2 + P_l^{*2})^{1/2}/T_c\right], \tag{90}$$

which arises from the product of the distribution functions for quarks and antiquarks.

In Eq.(90), $P_l^* = M_\perp \sinh Y^*$ is the longitudinal momentum of a dilepton in the plasma rest frame. The Boltzmann factor leads to the following correlation in the spectrum of dileptons produced in equilibrium QGP: the lepton pair distributions over $P_\perp$ (over M) become harder with increasing longitudinal dilepton momentum P_l^* observed in the CMS; i.e., the relative part of high values of transverse momenta (masses) increases. Indeed, an analysis of Eq.(90) readily shows that dilepton distributions over $P_\perp$ and M are distinct for distinct P_l^* values. In selection of events with high P_l^* values in these distributions, the fraction having high mass and $P_\perp$ values increases.

The observed longitudinal momentum of dileptons produced in the QGP model is determined both by the local value of the momentum P_l^* and by the hydrodynamic QGP expansion $P_l = M_\perp \sinh(Y^* + \chi)$. For large transverse dilepton mass $M_\perp$, the characteristic «thermal» rapidity value Y^* will be much lower than the values acquired under hydrodynamic expansion. The observed longitudinal momentum P_l will therefore not be related to P_l^*, and thus the «thermal» $P_\perp - P_l(M - P_l)$ correlations will be absent. For small $M_\perp$ the
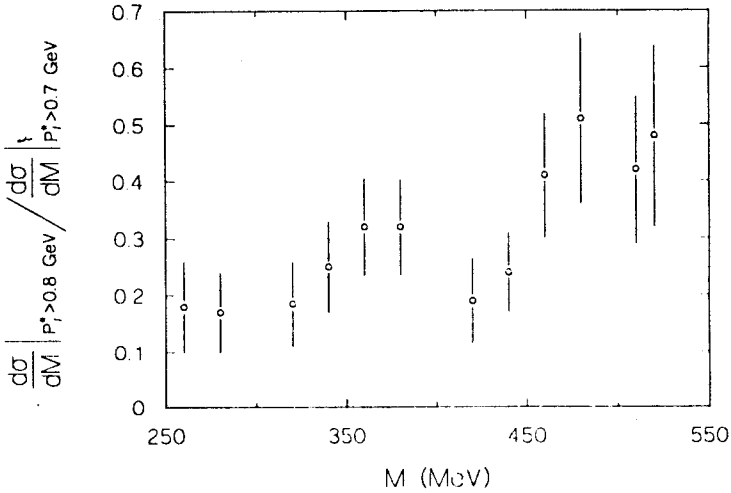
Fig.26. Ratio of dimuon mass spectra measured at different CMS longitudinal momenta P_l^* .

situation is vice versa. In this case, selection of events with large P_l effectively selects dileptons with large P_l^*, and indicated correlations occur. Such $P_\perp - P_l$ correlations are absent in the spectra of dileptons produced in pure hadronic processes [123]. An example of experimentally observed $M - P_l$ correlations may be a difference in the mass distributions of «anomalous» dimuons measured for different values of $x = 2P_l/\sqrt{s}$ [124, 125, 126]. This difference is shown in Fig.26. The part of the events with large mass increases with increasing longitudinal momentum P_l. Such an effect in heavy-ion collisions may be an indication of the existence of local thermodynamic equilibrium.

4.7. Ratio for Dilepton and Pion Spectra. Great progress has been made in the removal of uncertainties in QGP-driven dilepton spectra normalization by concrete bounds on thermalization times τ_i. This process is contingent upon entropy being conserved during the system evolution (section 3). The idea is to construct a τ_i independent quantity from experimentally observed spectra [22, 127,128]. Integrating over dilepton transverse momenta, we find from Eq.(34) the number of dileptons dN^{ll}/dy produced per unit rapidity. The quantity
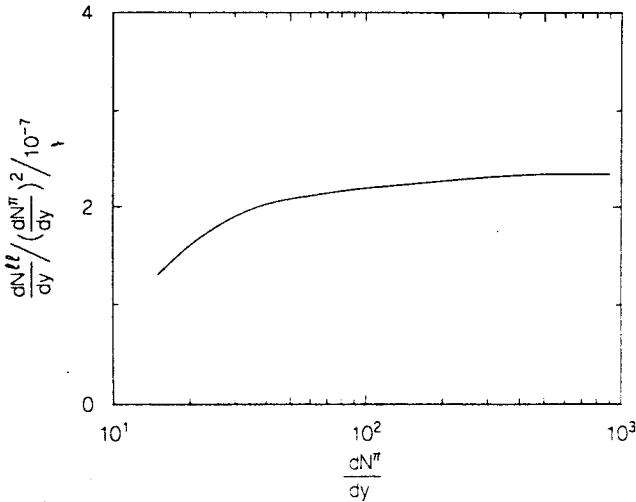
Fig.27. Ratio of dimuon and pion spectra

dN^{ll}/dy is proportional to τ_i^2 and to the multiplicity of charged pions dN^{π}/dy which is in turn proportional to τ_i. Therefore the ratio $(dN^{ll}/dy)/(dN^{\pi}/dy)^2$ does not depend on τ_i. This ratio is presented in Fig.27 [22].

The ratio turns out to be a monotonically increasing function of dN^{π}/dy if there exists only a pion phase in the thermalized state. If the initial energy density exceeds the QGP critical value (sections 2 and 3), this ratio goes to a plateau. The plateau height is proportional to the phase transition temperature T_c. The reason can be traced to the evolution of the nuclear matter. The system lives at a higher average temperature as T_c is increased, even though the duration is the same. Of course, the precise height of the plateau is complicated by effects not considered in the Bjorken model. For example, the transverse expansion would reduce the height of the plateau. There is also some sensitivity to the break-up temperature T_f, where pions lose mutual thermal contact.

But in any region of (pion) multiplicity, a measurement of the ratio $(dN^{ll}/dy)/(dN^{\pi}/dy)^2$ as a function of dN^{π}/dy seems to be of great importance from the viewpoint of a possible diagnostic of QGP formation in heavy-ion collisions.

4.8. Uncertainties in QGP and Hadron Gas Signals. The uncertainties in the values of τ_i and the initial QGP volume lead to considerable uncertainty in

Fig.28. The invariant mass spectrum of dilepton production from quark-antiquark annihilation during the plasma expansion in Au + Au collisions at 100 + + 100 GeV/nucleon, calculated with Bjorken expansion model in «hot-glue» (solid line) scenario and «standard» (dashed line) scenarios
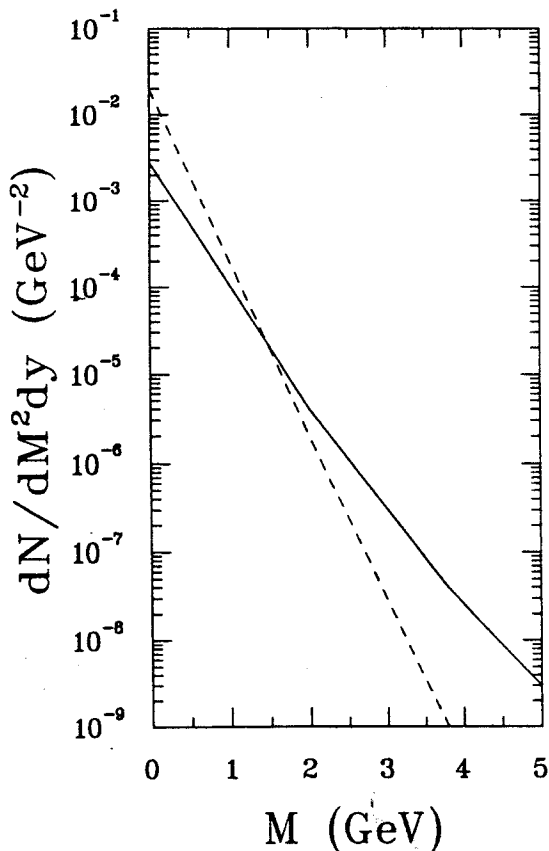
the estimation of the quark and hadronic phase contributions to the dilepton spectrum. Quite obviously, the quark phase constribution is enhanced for $\tau_i = 0.1$ fm/c, while the hadron phase contribution for $\tau_i \to 10$ fm/c.

As an illustration, we can again return to Figs.20 and 21. From these figures it is seen that the pion phase dominates over the quark phase in the region $M < < 2$ GeV for $\tau_i = 1$ fm/c. The quark component becomes noticeable for $M \geq 2$ GeV, again because quarks and antiquarks annihilate at higher temperatures than pions. If τ_i approaches 0.5 fm/c, then the quark component starts dominating over the hadronic one in the dilepton spectra for $M < 2$ GeV also. Thus, the exact form of dilepton spectrum cannot be predicted *a priori* for real experiments. Everything is ultimately determined by the relationship between the lifetimes of the two phases.

In section 3 we mentioned a «hot-glue» scenario of nuclear evolution. Remember, that in this scenario the gluons are thermalized at $\tau_g \simeq 1/2$ fm/c, but quarks have $\tau_q \simeq 2$ fm/c. Figure 28 shows the invariant mass dilepton spectra for «hot-glue» ($\tau_i = 0.3$ fm/c, $T_i = 460$ MeV) as the solid line and for «standard» scenarios ($\tau_i = 1$ fm/c, $T_i = 240$ MeV) as the dashed line [129]. One can
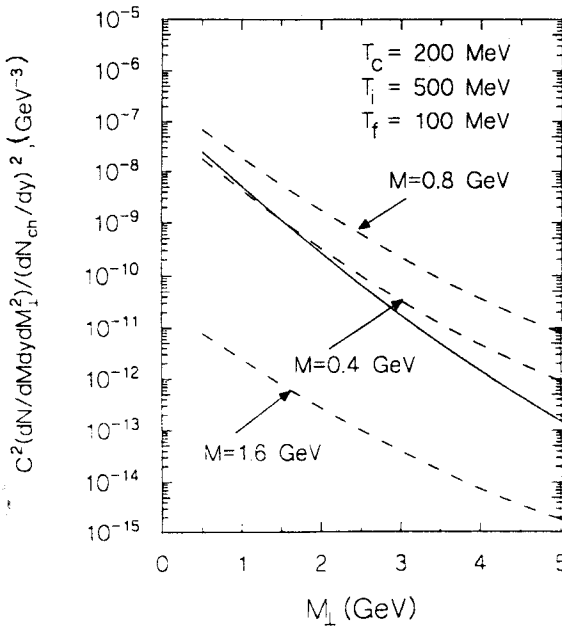
Fig.29. Transverse mass distributions without transverse flow

conclude that in the window $M \simeq 2$—3 GeV the «hot-glue» scenario leads to a dilepton yield exceeding the «standard» scenario prediction.

So far we discussed only a one-dimensional picture for evolution of the hadronic matter. But really the evolution is one-dimensional only in the QGP phase and the hadron gas as long as T is near T_c. At a temperatures $T \simeq T_f$ the evolution is probably closer to 3-dimensional [130]. The effects of transverse collective flow have been found to be important in the late stages of heavy-ion collisions [84,131,132,133]. Let us consider the dependence of dilepton production rates on the transverse mass of the pair $M_\perp$ and on the transverse flow of the matter. In Fig.29 transverse mass distributions from a calculation without transverse flow are shown [134] separately for the QGP (solid line) and hadron gas contributions at $M = 0.4$, 0.8, 1.6 GeV. As one can see from Fig.29, in the case of no transverse flow, the QGP contribution depends only on $M_\perp$ but not separately on the pair mass M. The hadron contribution has a strong M-dependence from the form factor. It is also clear that the slope of the hadron contribution is much larger than the QGP contribution. Without transverse flow

the steepness of the spectrum directly reflects the temperature of the emitting matter. In Fig.30, curves [134] for the same collection of parameters are shown when transverse flow is included. One concludes that transverse flow does not lead to large quantitative changes in the QGP contribution to dilepton spectra. However the effect of the transverse flow on the hadron contributions is profound in two ways. Firstly, the low $M_\perp$-part of the spectra is very strongly reduced. Secondly, the transverse flow enhances the production of large transverse mass pairs.

Let us return now to photon production. There may be a $p_\perp$ window span-

Fig.30. Transverse flow included

ning the transverse region from 2 to 4 GeV where thermal photons from the QGP might dominate since decay photons dominate at low $p_\perp$ and direct (hard QGP) photons dominate at larger $p_\perp$ [135,136,137]. But this conclusion ignores the transverse expansion of hadronic matter during its evolution. It is clear that the transverse expansion of the plasma becomes important in the later stages of the dynamics. The transverse flow effects on high energy photons emitted by expanding QGP were carefully analysed in Ref.[138]. At SPS and RHIC energies, the transverse flow of the hadronic matter is shown to completely close the $p_\perp$-window where photons from the quark matter dominate over those from the hadronic matter. At LHC energies, photons having a $p_\perp$ larger than about 4 GeV are shown to have their origin predominantly in the QGP. The location of the $p_\perp$ window is very sensitive to the value of the freeze-out temperature T_f. This temperature can in principle be obtained by comparing the dimensions of the system with the mean free path of hadronic matter consisting
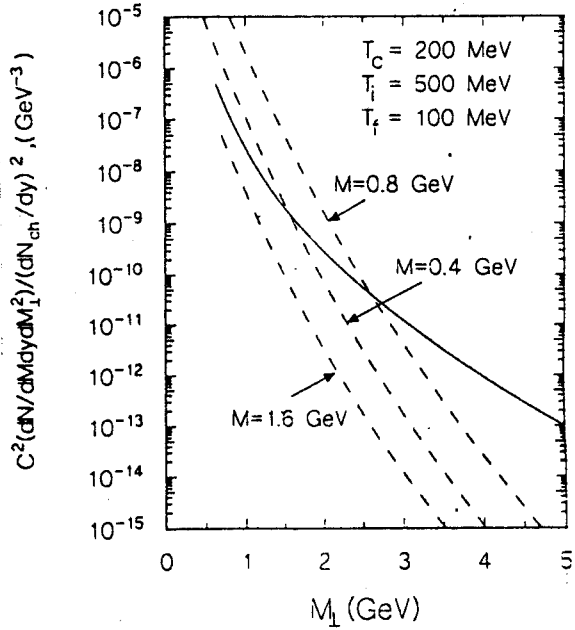
of π, ρ, ω and η mesoms. As in the case of dilepton production, we expect that the sensitivity of the results on the freeze-out temperature can perhaps be eliminated by adding a contribution from a gas of free-streaming hadrons [88].

Thus, the transverse expansion will generally not influence the production rates calculated in the pure quark and in the mixed phase. The most important changes would be expected when the system reaches the hadronic phase.

4.9. Quark-Gluon Plasma Versus Hadronic Gas: Single Photons. A self-consistent, lowest-order calculation of the real photon emission rate at fixed temperature T, using Braaten and Pisarski resummation techniques [139,140], has recently been carried out [111,141]. The result is

$$\omega \frac{dR}{d^3\vec{k}} = \frac{\alpha\alpha_s}{3\pi^2}T^2 \exp(-\omega/T)\left[\log\frac{\omega T}{m_\beta^2} + c\right],$$

where

$$m_\beta^2 = \frac{2\pi}{3}\alpha_s T^2, \quad c = 1.62.$$

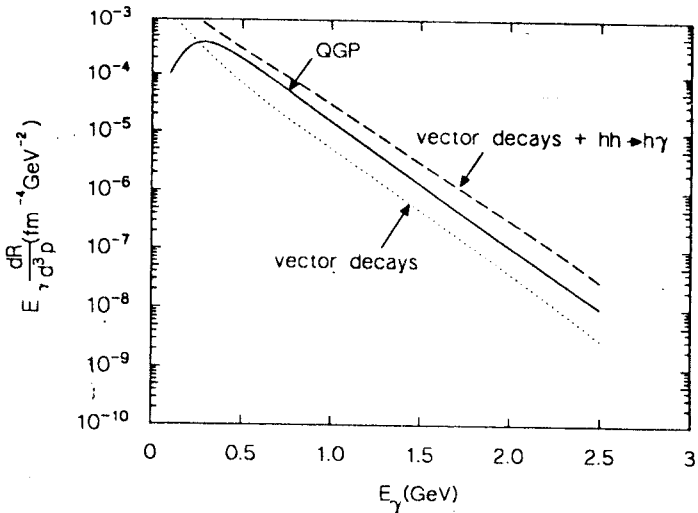Applying this to a nucleus-nucleus collision, one folds it at fixed temperature with final state expansion.

Fig.31. Comparison among photon production from quark-gluon plasma, from vector meson decay and from vector meson decay plus hadron reactions ($T = 200$ MeV)

Fig.32. The $\gamma\gamma$ mass distribution in the QGP (dashed and dotted lines) and hadronic gas (full line) at different T_i, T_c, T_f
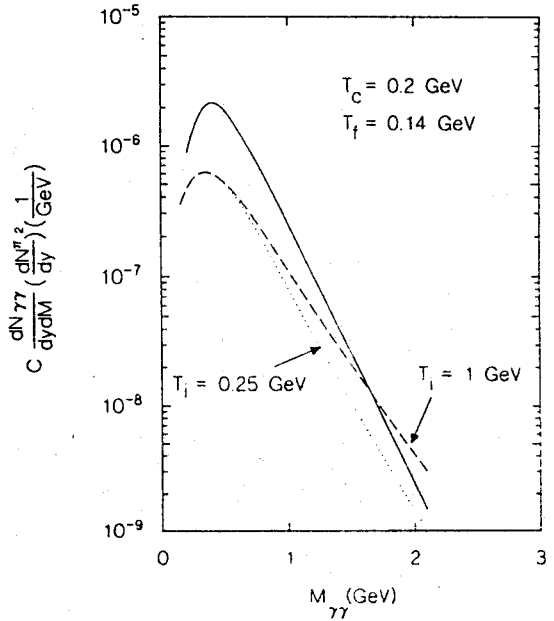
A careful analysis of photon emission from an hadronic gas has been done in Ref.[111]. The dominant contribution comes from the reactions $\pi\pi \to \rho\gamma$ and $\pi\rho \to \pi\gamma$; the decays $\omega \to \pi\gamma$ and $\rho \to \pi\pi\gamma$ are also important. Photon production rates at $T = 200$ MeV are shown in Fig.31 [111]. As one can see, the quark-gluon plasma and the hadronic gas produce photons with energies from 1 to 3 GeV at roughly the same rate. As was stressed in Ref.[111], not only is the shape of the production curve the same, but so is the overall magnitude. This means the photon spectrum is a good «thermometer» in heavy-ion collisions, but any temperature deduced from the thermally produced photons is nearly independent of assumptions about the phase of the matter [142]. If the QGP-hadron phase transition is first order, nuclear matter spends a long time at $T = T_c$ and consequently, most thermally produced photon will come from nuclear matter at T_c. This would allow us to determine T_c.

Based on the results of Ref.[111], it does not seem likely that photons with energies of 1 to 3 GeV will allow for distinguishing quark from pion degrees of freedom.

4.10. Photon Interferometry. The disadvantage of diphotons is that, as we have already seen, the cross sections for these processes are much lower than for single photon production. Indeed, the processes $q + \bar{q} \to \gamma\gamma$ and $\pi^+\pi^- \to \gamma\gamma$ are suppressed relative to the processes $gq \to q\gamma$, $q\bar{q} \to \gamma g$ for single proton production by a factor $\alpha = 1/137$. But these are important channels to consider in QGP diagnostics. Figures 32 and 33 show [118] the separate contributions to the diphoton spectrum coming from pions and from quark-antiquark annihilation at different values T_i, T_c, T_f. In the low-invariant mass region $M < 1.5$ GeV the

The y-axis is labeled $C \frac{dN_{\gamma\gamma}}{dydM} \left(\frac{dN^{\pi}}{dy}\right)^2 \frac{1}{(\text{GeV})}$

$T_i = 0.5$ GeV
$T_c = 0.2$ GeV
$T_f = 0.1$ GeV

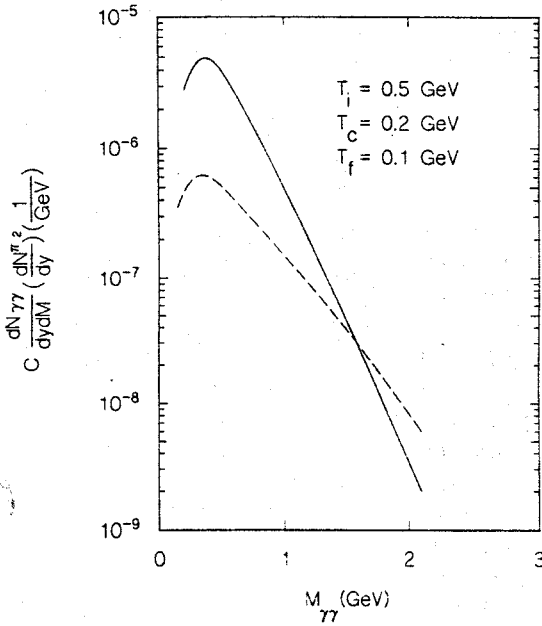The x-axis is labeled $M_{\gamma\gamma}$ (GeV)

Fig.33. Same as Fig.32 but for different temperatures

hadron contribution dominates diphoton production completely, even for rather large initial temperature $T_i \simeq 1$ GeV. For relatively low T_i the hadronic gas dominance is shifted to a higher value of M. For $T_i = 250$ MeV (even for $M = 4$ GeV) the QGP contribution is only about factor of 2 larger than the hadronic gas. When the initial temperature increases to 1 GeV (still at $M = 4$ GeV) the QGP contribution is already 3 orders of magnitude larger than pion gas.

The interesting possibility of probing the dynamics of quarks and gluons in a high energy nucleus-nucleus collisions using diphoton data has been noted in Ref.[86]. This method is based on two-photon intensity interferometry[143]. The correlation function between two photons with momenta $\vec{k}_1$ and $\vec{k}_2$ with the same helicity is

$$C(\vec{k}_1, \vec{k}_2) = \frac{P(\vec{k}_1, \vec{k}_2)}{P(\vec{k}_1)P(\vec{k}_2)} , \tag{91}$$

where

$$P(\vec{k}) = \int d^4x \, \frac{dN(x, \vec{k})}{d^4x \, d^3\vec{k}},$$

$$P(\vec{k_1}, \vec{k_2}) = \int d^4x_1 d^4x_2 \, \frac{dN(x_1, \vec{k_1})}{d^4x \, d^3\vec{k_1}} \, \frac{dN(x_2, \vec{k_2})}{d^4x_2 \, d^3\vec{k_2}} \, [1 + \cos(\Delta k \Delta x)] \qquad (92)$$

and $dN(x, \vec{k})/d^4x \, d^3\vec{k}$ is the rate per unit volume for producing a photon with momentum $\vec{k}$ at the space-time point x. The thermal emission rate of photons has been studied in Ref.[111]. It was found that the rates in the hadronic and plasma phases are the same when compared at the same temperature T

$$E \frac{dN}{d^4x \, d^3\vec{k}} = K_0 T^2 \ln\left(\frac{2.9E}{g^2T} + 1\right) \exp\left(-\frac{E}{T}\right), \qquad (93)$$

where E is the photon energy, g is the QGP coupling constant, and K_0 is a constant which is irrelevant to the correlation function. In Bjorken model of evolution, with photon momenta $k_{1T} = k_{2T} = k_T$ and rapidities $y_1 = y_2$, the correlation function is [86]

$$C(\vec{k_1}, \vec{k_2}) = 1 + \left[\frac{2J_1(q_T R)}{q_T R}\right]^2, \qquad (94)$$

where $q_T = k_T(\cos\psi_1 - \cos\psi_2)$ and ψ_1 and ψ_2 are the azimuthal angles of the photons. It is clear, that this photon configuration allows us to infer the radius R of the emitting system. Figures 34, 35 and 36 show [86] the correlation functions from the plasma, mixed and hadronic phases separately. The numbers next to the curves denote the individual photon transverse momentum in GeV/c. The correlation functions oscillate with varying Δy scale. But the Δy period is larger for the plasma by an order of magnitude over that the mixed or hadronic phases. Physically this means that the time scale in the plasma is much shorter than the time scale in the mixed or hadronic phases. So, with this configuration for the photons, the correlation
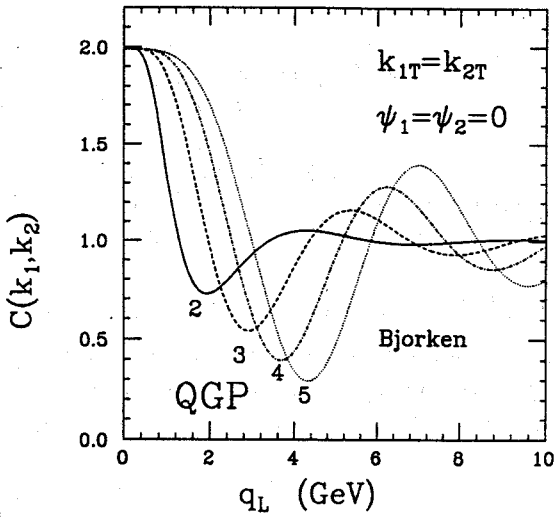
Fig.34. Correlation function at RHIC energy from the QGP phase. The numbers 2, 3, 4 and 5 indicate the transverse momentum of a single photon in GeV/c
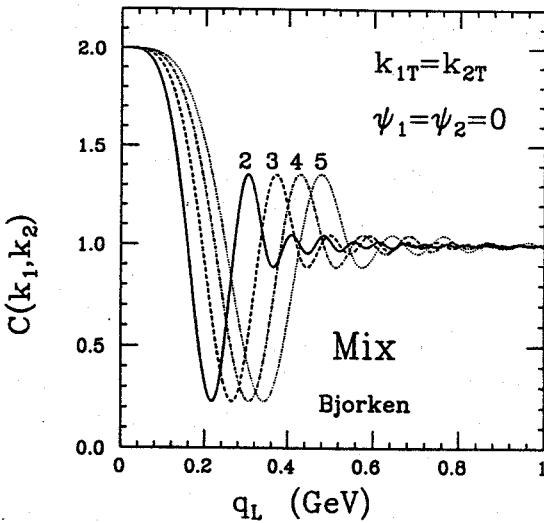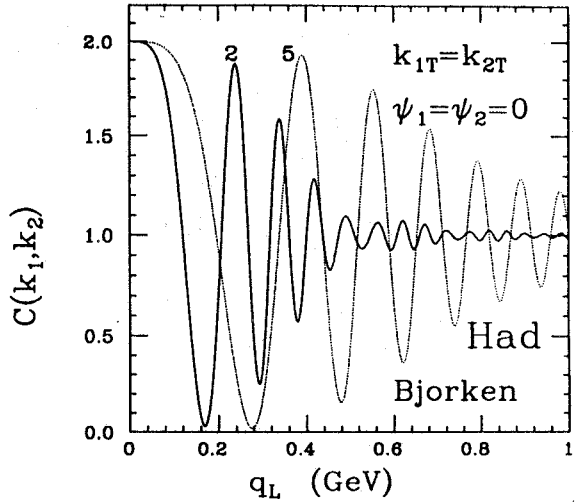

Fig.35. Correlation function at RHIC energy from the mixed phase and hadronic phase are added together

Fig.36. Correlation function at
LHC energy for hadronic phase

function $C(\vec{k_1}, \vec{k_2})$ is probing the temporal scale of the emitting source. Of course, the background from π_0 and η decays might destroy the beautiful tool of photon interferometry. It is also not clear whether the transverse expansion of matter in the mixed and final (hadronic) phases was small enough so that soft photons would not be boosted to high transverse momentum — different models [144,145] give the different answers — but there is no doubt that the method of intensity interferometry may give information about the space-time dynamics of quark and gluons in heavy-ion collisions.

4.11. Combinations of Dilepton, Photon, and Diphoton Spectra. Dilepton, photon and diphoton spectra depend on the (not so accurately known) thermalization time τ_i and on the initial volume. One way to circumvent this problem is to construct τ_i independent quantities from experimentally observed spectra $dN^{ll}/dM^2dyd^2\vec{q}_\perp$, $dN^\gamma/dyd^2p_\perp$ and $dN^{\gamma\gamma}/dMdyd^2p_\perp$.

In Fig.(37) [84], we show a plot of the ratio

$$R = \frac{dN^{\mu^+\mu^-}}{dM^2dyd^2p_\perp} \bigg/ \frac{dN^\gamma}{dyd^2p_\perp} \tag{95}$$

for various values of T_i (in units of T_c) as a function of transverse mass $M_\perp$. This ratio turns out to be independent of the mixed phase beyond
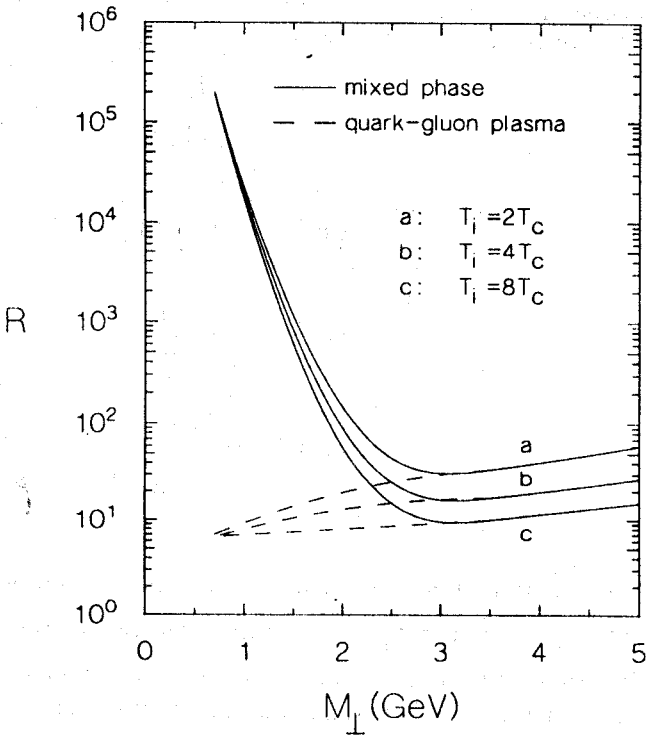
Fig.37. The ratio $\mu^+\mu^-/\gamma$ as a function of the initial temperatures ($M_\perp = q_\perp$ for photons)

$M_\perp \simeq 2$ GeV, saturating to a constant value for $T_i > 8T_c$. In Fig.38 [84,146] we plot the ratio

$$\frac{dN^{\mu^+\mu^-}}{dM^2 dy d^2 p_\perp} \bigg/ \frac{dN^{\gamma\gamma}}{dM^2 dy d^2 p_\perp} \tag{96}$$

as a function of mass for fixed dilepton and diphoton transverse momenta. The ratio is rather insensitive to $p_\perp$, reflecting the fact that the production processes for $\mu^+\mu^-$ and $\gamma\gamma$ are similar [84]. The ratio is independent of M beyond $M \simeq 10T_c$ ($\simeq 2$ GeV) and the dip corresponds to the sharp increase in e^+e^- cross section due to ρ-peak.
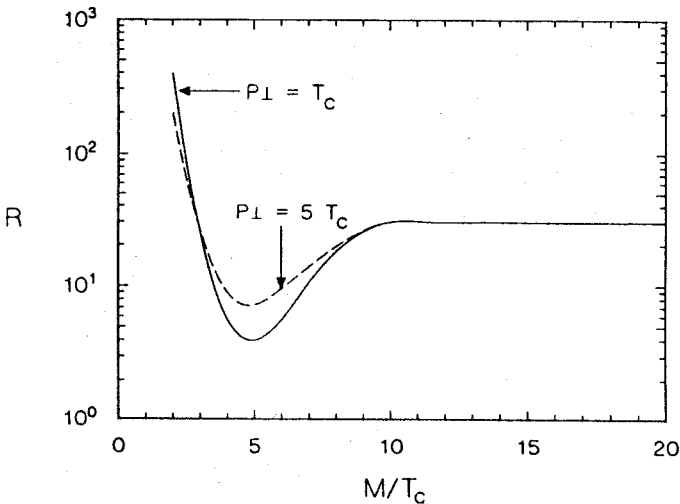
Fig.38. The ratio $\mu^+\mu^-/\gamma\gamma$ as a function of mass for transversely explanding QGP and hadronic gas

5. CONCLUSION

Dileptons and photons provide natural tools for observing high density nuclear matter, which one can form in relativistic heavy-ion collisions. Once produced, dileptons and photons hardly interact and collide infrequently, if at all, with hadrons in a region of hot and dense matter. Therefore, photons and lepton pairs are among the best carriers of information about the earliest stages of the heavy-ion collision. As we discussed in this review, they can carry information about the temperature of the primordial state. Such primordial states in high energy heavy-ion collisions could be equilibrium or non-equilibrium quark-gluon plasma, high density hadronic gas. That there are many competing sources of photons and dileptons both before and after the hot stage of the collision makes reconstruction of the hottest state very difficult. The best that one can do is to evaluate the contribution from each to ascertain whether or not it is dominant in some part of the phase space or if it has distinct properties rendering separation feasible. We tried to follow to this prescription in this paper. It is not clear that the first generation of CERN experiments has been able to produce quark-gluon plasma. However from the observed pion multiplicity of the order of a few hundreds, it is clear that these collisions are able to produce macroscopic drops of hot hadronic matter mainly made of pions in the temperature range 100—200 MeV. As we discussed in this review,

ρ, ϕ, J/ψ change its properties in hot nuclear matter. CERN experiments have shown that indeed these mesons change its properties in heavy-ion collisions. The modification of mesons properties were observed in its dilepton decay channel. The future experiments at RHIC and LHC to measure the dilepton and photon spectrum provide good and probably the only opportunity to verify experimentally the predicted properties of mesons in dense nuclear matter and clarify the nature of primordial state in heavy-ion collisions.

References

1. Shuryak E. — Phys. Reports, 1980, vol.67, p.71; **Shuryak E.** — Phys. Reports, 1984, vol.115, p.153.
2. Fermi E. — Progress in Theoretical Physics, 1950, vol.5, p.570.
3. Pomeranchuk I. — Doklady Akad. Nauk SSSR, 1951, vol.78, p.889.
4. Landau L. — Izvestija AN SSSR Ser. Fiz., 1953, vol.17, p.51; Collected Papers of Landau, Gordon and Breach, 1965, No.4.
5. Polyakov A. — Phys. Lett., 1979, vol.B82, p.247.
6. Susskind L. — Phys. Rev., 1979, vol.D20, p.2610.
7. Engels J. et al. — Nucl. Phys., 1982, vol.B205, p.595.
8. Morley P., Kislinger M. — Phys. Reports, 1979, vol.51, p.65.
9. Bjorken J. — Phys. Rev., 1983, vol.D27, p.140.
10. Hwa R., Kajantie K. — Phys. Rev. Lett., 1986, vol.56, p.696.
11. Koch P., Müller B., Rafelski J. — Phys. Reports, 1986, vol.142, p.1.
12. Lee K., Rhoades-Brown M., Heinz U. — Phys. Rev., 1988, vol.C37, p.1452.
13. Eggers H., Rafelski J. — GSI Preprint GSI-90-37, 1990.
14. Van Hove L. — Phys. Lett., 1982, vol.B118, p.138.
15. Greiner C., Koch P., Stöcker H. — Phys. Rev. Lett., 1987, vol.58, p.1825.
16. Feinberg E. — Proc. Kiev Conf. in High Energy Physics, 1959, vol.2.
17. Feinberg E. — Nuovo Cimento, 1976, vol.A34, p.39.
18. Shuryak E. — Sov. J. Nucl. Phys., 1978, vol.28, p.408.
19. Domokos G., Goldman T. — Phys. Rev., 1981, vol.D23, p.203.
20. Hwa R., Kajantie K. — Phys. Rev., 1985, vol.D32, p.1109.
21. McLerran L. Toimela T. — Phys. Rev., 1985, vol.D31, p.545.
22. Kajantie K. et al. — Phys. Rev., 1986, vol.D34, p.2746.
23. Braaten E., Pisarski R., Yuan T. — Phys. Rev. Lett., 1990, vol.64, p.2242.
24. Ruuskanen P. — Nucl. Phys., 1990, vol.A525, p.255.
25. Gale C., Kapusta J. — Phys. Rev., 1987, vol.C35, p.2107.
26. Xiong L. et al. — Nucl. Phys., 1990, vol.A512, p.772.

27. **Cassing W. et al.** — Phys. Reports, 1990, vol.188, p.363.

28. **Wilson K.** — Phys. Rev., 1974, vol.D10, p.2445.

29. **Creutz M.** — Phys. Rev., 1980, vol.D21, p.1006.

30. **Creutz M.** — Quarks, Gluons and Lattices, Cambridge Univ. Press, 1983.

31. **Toussaint D.** — Preprint AZPH-TH/91-33.

32. **Fukugita M., Ukawa U.** — Phys. Rev. Lett., 1986, vol.57, p.503.

33. **Karsch F. et al.** — Phys. Lett., 1986, vol.B188, p.353.

34. **Gottlieb S. et al.** — Phys. Rev., 1987, vol.D35, p.3972.

35. **Brown F. et al.** — Phys. Lett., 1990, vol.B251, p.181.

36. **Fukugita M. et al.** — Phys. Rev. Lett., 1990, vol.65, p.816.

37. **Kogut J., Sinclair D.** — Phys. Lett., 1989, vol.B229, p.807.

38. **Brown F. et al.** — Phys. Rev. Lett., 1990, vol.65, p.2491.

39. **Pisarski R., Wilczek F.** — Phys. Rev., 1984, vol.D29, p.338.

40. **Gottlieb S. et al.** — Phys. Lett., 1987, vol.59, p.1513.

41. **Gottlieb S. et al.** Phys. Rev., 1990, vol.D41, p.622.

42. **Bitar K. et al.** — Phys. Rev. Lett., 1990, vol.65, p.2106.

43. **Grady M., Kogut J., Sinclair D.** — Phys. Lett., 1988, vol.B200, p.149.

44. **Gavai R. et al.** — Phys. Lett., 1990, vol.B241, p.567.

45. **Emel'yanov V., Nikitin Yu., Vanyashin A.** — Fortschritte der Phys. 1990, vol.38, p.1.

46. **Satz H.** — Preprint CERN-TH-6216/91.

47. **Karsch F., Wyld H.** — Phys. Lett., 1988, vol.B213, p.505.

48. **Engles T. et al.** — Bielefeld Preprint BI-TH-29/90, 1990

49. **Petersson B.** — Bielefeld Preprint BI-TP-90/28, 1990.

50. **De Tar C., Kogut J.** — Phys. Rev. Lett., 1987, vol.59, p.399.

51. **Irbäck A.** — Bielefeld Preprint BI-TP-90/44, 1990.

52. **Sumiyoshy H. et al.** — Z. Phys., 1984, vol.C23, p.391.

53. **Van Hove L.** — Z. Phys., 1983, vol.C21, p.93.

54. **Cerny V., Lichard P., Pisut J.** — Phys. Rev., 1977, vol.D16, p.2822.

55. **Cerny V., Lichard P., Pisut J.** — Phys. Rev., 1978, vol.D18, p.2409.

56. **Cerny V., Lichard P., Pisut J.** — Phys. Rev., 1979, vol.D20, p.699.

57. **Kajantie K., Matsui T.** — Phys. Lett., 1985, vol.B164, p.373.

58. **Baym G.** — Phys. Lett., 1984, vol.B138, p.18.

59. **Geiger K., Müller B.** — Nucl. Phys., 1992, vol.B369, p.600.

60. **Geiger K.** — Phys. Rev., 1992, vol.D46, p.4965.

61. **Geiger K.** — Phys. Rev., 1992, vol.D46, p.4986.

62. **Shuryak E.** — Phys. Rev. Lett., 1992, vol.68, p.3270.

63. **Satz H.** — Nucl. Phys., 1992, vol.A544, p.371c.

64. **Capella A.** — Nucl. Phys., 1991, vol.A525, p.133c.
65. **Sakharov A.D.** — Sov. JETP Lett., 1967, vol.5, p.32.
66. **Chodos A. et al.** — Phys. Rev., 1974, vol.D9, p.3473.
67. **Letessier J., Tounsi T.** — Phys. Rev., 1989, vol.D40, p.2914.
68. **Gorenstein M., Zinovjev G., Lipskikh S.** — Z. Phys., 1984, vol.C22, p.189.
69. **Landau L.** — Izv. Akad. Nauk SSSR, ser. fiz., 1953, vol.17, p.51.
70. **McLerran L.** — Phys. Reports, 1982, vol.88, p.379.
71. **Carruthers P.** — Annals of Physics, 1974, vol.229, p.91.
72. **Anishetty R. et al.** — Phys. Rev., 1980, vol.D22, p.2793.
73. **Milekhin G.** — In.: Proc. Int. Cosmic Ray Conf., Moscow, 1959, vol.1, p.220.
74. **Chin C. et al.** — Phys. Rev., 1975, vol.D12, p.902.
75. **Satz H.** — In: Proc. of 1st Meeting on Heavy-Ion Physics at LHC, Geneva, February, 1991.
76. **Danielewicz P., Gyulassy M.** — Phys. Rev., 1985, vol.D31, p.53.
77. **Hosoya A. et al.** — Annals of Physics, 1984, vol.154, p.229.
78. **Chu M.** — Phys. Rev., 1986, vol.D34, p.2764.
79. **Biagini M.E., Dubnicka S., Etim E., Kolar P.** — Nuovo Cimento, 1991, vol.A104, p.363.
80. **Zhirov O.** — Sov. J. Nucl. Phys., 1979, vol.30, p.1098.
81. **Domokos G., Goldman J.** — Phys. Rev., 1981, vol.D23, p.203.
82. **Hwa R., Kajantie K.** — Phys. Rev., 1986, vol.D32, p.1109.
83. **Masarik J., Pisutova N., Pisut J.** — Phys. Lett., 1991, vol.B254, p.474.
84. **Raha S., Sinha B.** — Int. Journal of Mod. Phys., 1991, vol.A6, p.517.
85. **Csernai L., Kapusta J.** — Phys. Rev. Lett., 1992, vol.69, p.737.
86. **Srivastava D., Kapusta J.** — Preprint TPI-MINN-93/8-T.
87. **Kapusta J., Lichard P.** — Phys. Rev., 1989, vol.C40, p.R1574.
88. **Kapusta J., McLerran L., Srivastava D.** — Phys. Lett., 1992, vol.B283, p.145.
89. **Altherr T., Aurech P., Becherrawy T.** — Nucl. Phys., 1989, vol.B315, p.436.
90. **Altherr T., Becherrawy T.** — Nucl. Phys., 1990, vol.B330, p.174.
91. **Baier R., Pire B., Schiff D.** — Phys. Rev., 1988, vol.D38, p.2814.
92. **Braaten E., Pisarski R., Yuan T.** — Phys. Rev. Lett., 1990, vol.64, p.2242.
93. **Altherr T., Russkanen P.** — Preprint JYFT 7/92.
94. **Landau L., Pomeranchuck I.** — Dokl. Acad. Nauk SSSR, 1953, vol.92, p.535; 1953, vol.92, p.735.
95. **Schafer M. et al.** — Phys. Lett., 1989, vol.B221, p.1.
96. **Haglin K., Kapusta J., Gale C.** — Phys. Lett., 1989, vol.B224, p.433; **Haglin K.L.** — Annals of Physics, 1991, vol.212, p.84.
97. **Ruckl R.** — Phys. Lett., 1976, vol.B64, p.39.

98. Gale C., Kapusta J. — Phys. Rev., 1988, vol.C38, p.2659.

99. Wolf G. et al. — Nucl. Phys., 1990, vol.A517, p.615.

100. Low F.E. — Phys. Rev., 1958, vol.110, p.974.

101. Haglin K., Gale C., Emel'yanov V. — Phys. Rev., 1993, vol.D47, p.973.

102. Byckling E., Kajantie K. — Particle Kinematics, Wiley, New York, 1973, p.23.

103. Haglin K., Gale C., Emel'yanov V. — Phys. Rev., 1992, vol.D47, p.4082.

104. Gale C., Kapusta J. — Phys. Rev., 1989, vol.C40, p.2397.

105. Weinberg S. — Phys. Rev. Lett., 1966, vol.17, p.616.

106. Cleymans J., Redlich K., Satz H. — Z. Phys., 1991, vol.C53, p.517.

107. Cleymans J., Goloviznin V.V., Redlich K. — Phys. Rev., 1993, vol.D47, p.989.

108. Leader J., Predazzi E. — An Introduction to Gauge Theories and the «New Physics», Cambridge University Press, Cambridge, England, 1982.

109. Danielewicz P., Gyulassy M. — Phys. Rev., 1985, vol.D31, p.53.

110. DeGrand T., Toussaint D. — Phys. Rev., 1982, vol.D25, p.526.

111. Kapusta J., Lichard P., Seibert D. — Phys. Rev., 1991, vol.D44, p.2774; Phys. Rev., 1993, vol.D47, p.4171(E).

112. Sinha B. — Nucl. Phys., 1986, vol.A459, p.717.

113. Sinha B. — Phys. Lett., 1983, vol.B128, p.91.

114. Kajantie K. et al. — Nucl. Phys., 1983, vol.B222, p.152.

115. Chin S.A. — Phys. Lett., 1982, vol.B119, p.51.

116. Domokos G. — Phys. Rev., 1983, vol.D28, p.123.

117. Yoshida R. et al. — Phys. Rev., 1987, vol.D35, p.388.

118. Redlich K. — Phys. Rev., 1987, vol.D36, p.3378.

119. Ruuskanen P. — Nucl. Phys., 1991, vol.A525, p.255c.

120. Gale C., Lichard P. — Phys. Rev., 1994, vol.D49, p.3348.

121. Song C., Ko C.M., Gale C. — Phys. Rev., 1994, vol.D50, p.R1827.

122. Lichard P. — Phys. Rev., 1994, vol.D49, p.5812.

123. Fassler M. — Preprint CERN-EP/86-102.

124. Haber B. et al. Phys. Rev., 1980, vol.D22, p.2107.

125. Andersson K. et al. — Phys. Rev. Lett., 1976, vol.36, p.237.

126. Blokus D. et al. — Nucl. Phys., 1982, vol.B201, p.205.

127. Kampfer B., Gorenstein M., Pavlenko O. — Z. Phys., 1990, vol.C45, p.491.

128. Kampfer B., Pavlenko O. — Phys. Lett., 1991, vol.B255, p.503.

129. Shuryak E., Xiong L. — Phys. Rev. Lett., 1993, vol.70, p.2241.

130. Landau L., Lifshitz E. — Fluid Mechanics, Pergamon Press, Oxford, 1959.

131. Von Gersdorf H. et al. — Phys. Rev., 1986, vol.D34, p.794.

132. Kajantie K. et al. — Phys. Rev., 1986, vol.D34, p.811.

133. Letessier J., Tounsi A. — Phys. Rev., 1989, vol.D40, p.2914.

134. **Kataja M. et al.** — Preprint JYFL 1/92.

135. **Sinha B.** — Phys. Lett., 1983, vol.B128, p.91.

136. **Hwa R., Kajantie K.** — Phys. Rev., 1985, vol.D32, p.1109.

137. **Srivastava D., Sinha B.** — J. Phys., 1992, vol.G18, p.1467.

138. **Alam J., Srivastava D., Sinha B., Basu D.** — Phys. Rev., 1993, vol.D48, p.1117.

139. **Braaten E., Pisarski R.** — Phys. Rev. Lett., 1990, vol.64, p.1338.

140. **Braaten E., Pisarski R.** — Nucl. Phys., 1990, vol.B337, p.569.

141. **Baier R. et al.** — Preprint BI-TP 91/15, May 1991.

142. **Seibert D., Mishra V., Fai G.** — Phys. Rev., 1992, vol.C46, p.330.

143. **Hanbury Brown R.** — The Intensity Interferometry, Taylor&Francis, 1974.

144. **Kajantie K. et al.** — Phys. Rev., 1987, vol.D34, p.2153.

145. **Bertsch G. et al.** — Phys. Rev., 1989, vol.D37, p.1202.

146. **Datta B., Raha S., Sinha B.** — Nucl. Phys., 1988, vol.A490, p.733.